



Norwegian University of
Science and Technology

Study of wind turbine wake aerodynamics through vortex flow visualization

Erik Lie Gjesdal

Master of Energy and Environmental Engineering

Submission date: June 2017

Supervisor: Nicholas Worth, EPT

Norwegian University of Science and Technology
Department of Energy and Process Engineering

EPT-M-2017-25

MASTER THESIS

for

Erik Gjesdal

Spring 2017

*Study of wind turbine wake aerodynamics through vortex flow visualisation***Background and objective**

The use of wind energy is becoming increasingly widespread, and is likely to feature heavily in sustainable energy networks of the future. However, the complex aerodynamic performance of wind turbines result in significant challenges during their design and deployment. At present we do not fully understand the structure of the rotating wakes which are found downstream of wind turbines. This understanding is particularly important for the design of wind turbines, which are often clustered together in 'parks' or 'farms'. In such arrangements, the performance and fatigue life of a turbine is likely to depend on the characteristics of the wake flow from any upstream turbines, and therefore developing a complete understanding of the turbulent wake structure is crucial to their deployment and optimisation. This project will focus on setting up a novel experiment to investigate wake effects based on rotating and translating a simplified model turbine blades through a tank of water, and visualising the wake flow.

The project will involve the development of a Labview control code to translate and rotate the wings, and the testing of this code in the newly developed towing tank facility. Flow visualization will be conducted using high speed cameras and dye injected into the wake in order to visualize the vortex interactions.

The following tasks are to be considered:*Literature Review*

1. Background reading and literature review of wind turbine wakes, including: why studying these is of interest in a practical sense; the dominant structure of the wake and coherent motions within it; the formation of tip vortices; the role of tip vortices in modifying the turbulent structure of the wake
2. Background reading and literature review of tow tank studies, imaging and flow visualization methods.

Translating wing experiments

1. Develop a Labview script capable of traversing wing through the towing tank.
2. Conduct flow visualization study
3. Record flow visualisation using high speed cameras, and make analysis of flow structure.

Within 14 days of receiving the written text on the master thesis, the candidate shall submit a research plan for his project to the department.

When the thesis is evaluated, emphasis is put on processing of the results, and that they are presented in tabular and/or graphic form in a clear manner, and that they are analyzed carefully.

The thesis should be formulated as a research report with summary both in English and Norwegian, conclusion, literature references, table of contents etc. During the preparation of the text, the candidate should make an effort to produce a well-structured and easily readable report. In order to ease the evaluation of the thesis, it is important that the cross-references are correct. In the making of the report, strong emphasis should be placed on both a thorough discussion of the results and an orderly presentation.

The candidate is requested to initiate and keep close contact with his/her academic supervisor(s) throughout the working period. The candidate must follow the rules and regulations of NTNU as well as passive directions given by the Department of Energy and Process Engineering.


Risk assessment of the candidate's work shall be carried out according to the department's procedures. The risk assessment must be documented and included as part of the final report. Events related to the candidate's work adversely affecting the health, safety or security, must be documented and included as part of the final report. If the documentation on risk assessment represents a large number of pages, the full version is to be submitted electronically to the supervisor and an excerpt is included in the report.

Pursuant to "Regulations concerning the supplementary provisions to the technology study program/Master of Science" at NTNU §20, the Department reserves the permission to utilize all the results and data for teaching and research purposes as well as in future publications.

The final report is to be submitted digitally in DAIM. An executive summary of the thesis including title, student's name, supervisor's name, year, department name, and NTNU's logo and name, shall be submitted to the department as a separate pdf file. Based on an agreement with the supervisor, the final report and other material and documents may be given to the supervisor in digital format.

- Work to be done in lab (Fluids engineering lab)
 Field work

Department of Energy and Process Engineering, 15. January 2017



12/1/17

Nicholas Worth
Academic Supervisor

Research Advisor:

Preface

The work on this master thesis has been carried out at the Department of Energy and Process Engineering at the Norwegian University of Science and Technology (NTNU). All experimental work has been conducted at the Fluid Mechanics Laboratory.

The purpose of this thesis has been to assess the performance of the new blade Tow Tank Rig in the Fluid Mechanics Lab. The experimental work has been challenging, and also at times frustrating. However, in the end, it has been a great learning experience. I appreciate the opportunity to obtain hands-on lab experience and hope that the lessons learned during this semester are something I can bring with me in the years to come.

I would like to thank my supervisor Nicholas Worth. He has helped, encouraged and challenged me throughout the semester. His insights and suggestions helped guide me on the right path. I would also like to thank the technical staff at the Fluid Mechanics Lab, and especially Arnt Egil Kolstad, that helped me with equipment and technical fixes many times during the time spent in the lab. Finally, I would like to thank Jenny Marie Bjørnsgaard, who's work on her master thesis last year was a precursor to much of what I have done in my master thesis.

Abstract

In this master thesis, a flow visualization experiment and a blade tracking experiment have been conducted. The aim of the thesis has been to assess the performance of the new blade tow tank rig at the Fluid Mechanics Lab at NTNU. The blade tracking experiment involved reconstructing the trajectory of the blade and analyzing the blade's vibrations. The flow visualization experiment involved analyzing the tip vortices produced in the wake of the blade. This experiment is conducted by injecting dye into the tank near the tip of the blade.

A LabVIEW program has been created to accurately control the blade in the tank, through sending signals to the two stepper motors controlling the traversing and rotational motion of the blade. The program is designed to allow the user to quickly pick a specific velocity and acceleration of the blade, and thus a specific tip speed ratio (λ).

The blade tracking experiment was able to accurately reconstruct the trajectory of the blade. It also yielded some interesting results regarding the error associated with camera focus (depth of field). The results were, however, inconclusive regarding the nature of the blade vibrations. The flow visualization experiment produced images of the tip vortices at different values of λ . The expected result that is increasing λ decreases the strength of the tip vortices was also found, by comparing the change in intensity for the different scenarios.

The overall result of confirming the usability of the rig is important, because it opens up the possibility for many future research projects. By creating procedures for creating tip vortices as well as analyzing the trajectory of the blade, this thesis might prove to be an important step in much research in the years to come. Since the strength of the tip vortices is closely linked to the wake recovery length, the results from this thesis further proves the potential for improving wind farm efficiency. The results also proved the importance of high-quality imagery, as it turned out the cameras' frame rate and depth of field proved detrimental to the result of the blade tracking experiment.

Sammendrag

I denne masteroppgaven har et eksperiment innen styrømningsvisualisering, i tillegg har et eksperiment for sporing av et turbinblad blitt gjennomført. Hovedmålet for oppgaven har vært å vurdere ytelsen til et nybygd eksperimentalt sleppetankkannlegg ved strømningslabben på NTNU. Sporingseksperimentet gikk ut på å rekonstruere banen til et turbinblad, samt analysere bladets vibrasjoner. Visualiseringsseksperimentet gikk ut på å analysere virvelstrømningene i bladets vake. Dette ble gjennomført ved å injisere melk i strømmingen nær tuppen på bladet.

Et LabVIEW program har blitt lagd for å kunne kontrollere bladet i tanken. Dette gjøres ved å sende elektriske signaler til to steppermotorer. Programmet er lagd slik at brukeren enkelt kan spesifisere bladets hastighet og akselerasjon.

Resultatene fra sporingseksperimentet klarte med god nøyaktighet å rekonstruere bladets bane gjennom tanken. Resultatene visste også hvor stor påvirkning kameraenes fokus hadde på nøyaktigheten av målingene. Resultatene var likevel mangelfulle når det gjaldt å informasjon om bladets vibrasjoner. Visualiseringseksperimentet klarte å produsere gode bilder av virvelstrømningene ved ulike verdiene av λ . Eksperimentet fant også en forventet korrelasjon mellom økning i λ og minskning av styrken til virvelstrømningene.

Det overordnede resultatet, at riggen fungerte etter intensjonen, er viktig. Dette åpner opp muligheter for mange ulike forskningsprosjekter i fremtiden. Gjennom det faktum å finne enkle og gjennomførbare måter å produsere virvelstrømninger i bladets vake, samt rekonstruering av bladets bane, kan denne oppgaven vise seg å være viktig i årene som kommer. Resultatet som viser at styrken i vaken er korrelert med λ er ytterligere bevis for effektiviteten til vindparker kan forbedres ytterligere. Resultatene viste også viktigheten av gode kameraer, da manglende bildefrekvens og fokusdybde viste seg å være utslagsgivende for sporingseksperimentet.

Contents

Acknowledgment	i
1 Introduction	2
1.1 Background	2
1.2 Motivation	3
1.3 Previous Work	4
1.4 Problem Formulation	5
1.5 Structure of Thesis	6
2 Literary Study	7
2.1 Fundamental Principles in Wind Turbine Design	7
2.1.1 Actuator Disc Theory	7
2.1.2 Blade Element Momentum Theory	9
2.2 Wakes	12
2.2.1 Wake Effects	12
2.2.2 Wake Structure	13
2.3 Tip Vortices	14
2.4 Mitigating Losses	15
2.5 Flow Visualization	16
2.6 Starting Vortices	17
2.7 Camera Calibration	18
2.7.1 Pinhole Model	18
2.7.2 Camera Calibration Based on Polynomial Fitting	19

3 Methodology	21
3.1 Experimental Motivation	22
3.2 Dynamic Similarity	22
3.3 Blade Tow Tank Rig	24
3.3.1 The Tank	25
3.3.2 Stepper Motors	26
3.3.3 The Blade	27
3.3.4 The Camera	27
3.4 Labview Script	28
3.5 Blade Vibrations Experiment	31
3.5.1 Calibration Setup/ Plate	32
3.5.2 Blade Tracking	33
3.6 Flow Visualization Experiment	35
3.6.1 Calculating Flow Velocity	36
4 Results	39
4.1 Flow Visualization	40
4.1.1 Tip Vortices	40
4.1.2 Starting Vortices	44
4.2 Discussion Regarding Flow Visualization	45
4.2.1 Sources of error	45
4.3 Blade Vibrations Results	46
4.3.1 Path of Blade	46
4.3.2 Vibrations	47
4.3.3 Depth of Field Error	49
4.4 Discussion Regarding Blade Vibrations	50
5 Summary	52
5.1 Conclusion	52
5.2 Further Work	53
5.2.1 Water Quality	54

5.2.2 Blade Shape 54

5.2.3 Blade Vibration 54

5.2.4 Dye Injection 55

5.2.5 Future Research 55

Bibliography **55**

A Matlab Scripts **62**

A.1 Calculating Z-coordinate 62

A.2 MATLAB Scripts 62

A.3 Blade Tracking Data 65

A.4 MATLAB Scripts 65

B LabVIEW Block Diagram **77**

List of Figures

1.1	Global Wind Power Cumulative Capacity [1]	3
1.2	Wake at Horns Rev Wind Farm[2]	4
2.1	Actuator Disc [3]	8
2.2	Relative velocity [4]	9
2.3	Forces Acting on an Airfoil [5]	9
2.4	Wake development broken down into sections [6]	13
2.5	Tip vortices visualized using smoke [7]	14
2.6	Effective angle of attack for varying tip-speed ratio [8]	15
2.7	Osborne Reynolds' sketches of laminar to turbulent transition [9]	17
2.8	Important and interesting caption [10]	18
3.1	Blade Tow Tank Rig Schematic	24
3.2	Empty Tank	25
3.3	Stepper Motors	26
3.4	The Blade	27
3.5	Wake development broken down into sections	27
3.6	LabVIEW Flow Chart	28
3.7	LabVIEW Front Panel	29
3.8	Calibration plate in tank	31
3.9	Calibration Plate	32
3.10	Calibration Plate tilted	32
3.11	Line of sight of cameras intersecting at calibration plate	33

3.12 White dot on blade for blade tracking	34
3.13 Tube used for dye injection	35
4.1 Unprocessed Image	40
4.2 Proccesed Image	40
4.3 Strength of vortices	41
4.4 Aggregated Motion of tip Vortices	42
4.5 Intensity change between images	42
4.6 Aggregated Motion of tip Vortices	42
4.7 Intensity change between images	42
4.8 Aggregated Motion of tip Vortices	43
4.9 Intensity change between images	43
4.10 Aggregated Motion of tip Vortices	43
4.11 Intensity change between images	43
4.12 Aggregated Motion of tip Vortices	44
4.13 Intensity change between images	44
4.14 Starting vortices for $\lambda = 2.5$	44
4.15 Intensity change between images	44
4.16 Blade trajectory for $\lambda = 5$	46
4.17 Blade trajectory for $\lambda = 6$	46
4.18 Blade trajectory for $\lambda = 7$	47
4.19 Blade trajectory for $\lambda = 8$	47
4.20 Blade trajectory for $\lambda = 9$	47
4.21 Blade trajectory for $\lambda = 10$	47
4.22 Blade movement in z-direction for $\lambda = 5$	48
4.23 Blade movement in z-direction for $\lambda = 6$	48
4.24 Blade movement in z-direction for $\lambda = 7$	48
4.25 Blade movement in z-direction for $\lambda = 8$	48
4.26 Blade movement in z-direction for $\lambda = 9$	49
4.27 Blade movement in z-direction for $\lambda = 10$	49

4.28 Blade out of focus	49
4.29 Blade in focus	49
4.30 Error due to lack of focus	50
B.1 Signal Generation	77
B.2 Pulse in Loop	77
B.3 Acceleration Code	78
B.4 Safety Features	78
B.5 End of Cycle	79

Nomenclature

α Angle of Attack

λ Tip Speed Ratio

ρ Density

fps frames per second

NTNU Norwegian University of Science and Technology

Chapter 1

Introduction

1.1 Background

Over the course of the last several decades, the amount of installed capacity from wind energy has seen exponential growth. [1], as depicted in fig. 1.1. All over the world, wind turbines are being constructed in order to meet the growing demand for energy. Wind energy is increasingly becoming competitive with fossil fuels, due to drastically lowered cost [11]. Based on the current trajectory of wind energy, it seems likely that wind energy will play an important role in the energy solutions of the future. Norway is not exempt from this global trend. In the next couple of years, the building of Europe's largest onshore wind power project will take place in Fosen, which will eventually have a capacity of 1000 MW [12]. In fact, the new capacity of wind energy seems to be fairly evenly distributed throughout the world. Both in developed first world economies like the United States and Germany, as well as emerging markets such as China and India.

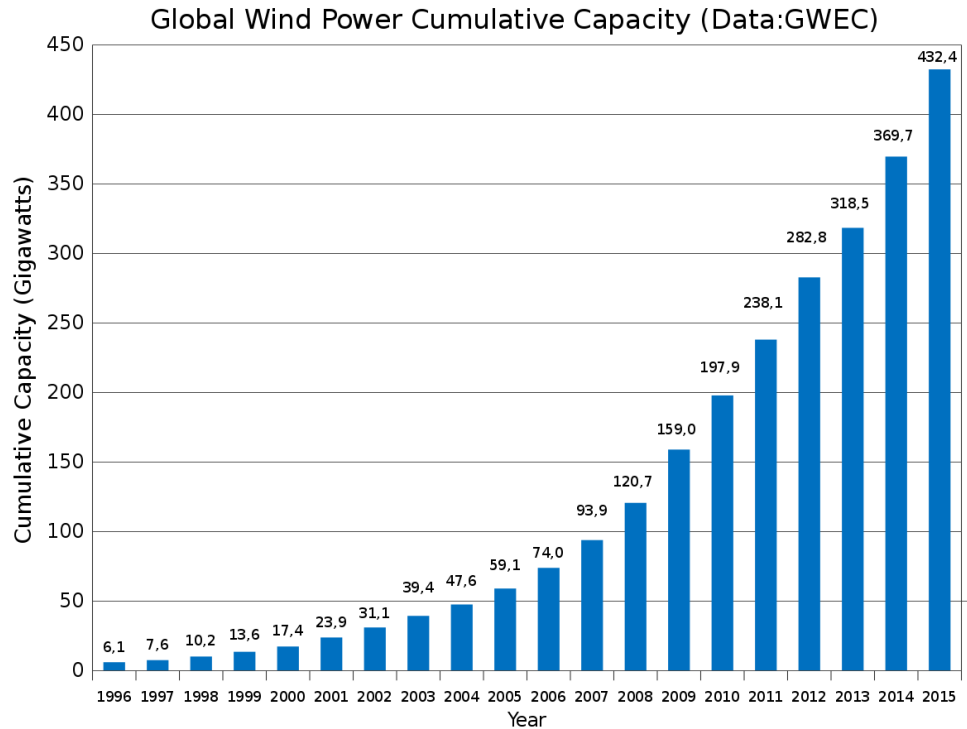


Figure 1.1: Global Wind Power Cumulative Capacity [1]

Another factor working in favor of wind energy are governmental incentives. Governments around the world have instituted policies that favor the production of electricity from wind, over non-renewable alternatives like coal and nuclear. Examples of this are the EU's renewable energy directive, that sets the ambitious goal of 20% of the EU's total energy to need to be renewable by 2020, as well as the German Energiewende [13] and the American Clean Power Plan. Although, the Clean Power Plan was recently revoked, and how that will turn out is an open question at this point [14]). However, many individual states (like California [15]) have set up their own incentive structure.

1.2 Motivation

In order to maximize profits from wind farms, turbines are generally ordered in an array structure, in what is known as wind farms. This allows for the maximum usage of a given area with favorable wind conditions. It also minimizes the area occupied by the turbines and its accom-

panying infrastructure (per turbine). Maintenance costs are also reduced by having the turbines in close proximity of one another.



Figure 1.2: Wake at Horns Rev Wind Farm[2]

However, organizing the turbines into wind farms causes some serious complications. Because of the fact that turbines are placed downstream of one another, they experience vastly different wind conditions. These differences in conditions are due to the fact that they are placed in the wake of other turbines [16]. This effect is clearly shown in fig. 1.2. Understanding this effect could yield higher wind farm power output, lower maintenance cost, and thus, more profitable wind farms. It is worth noting that the wake is usually invisible to the naked eye, specific conditions were needed in order for the situation one can see in fig. 1.2 to arise.

1.3 Previous Work

Wind turbine wakes have been a study of interest for about as long as there has existed industrial size wind farms. Researchers have gone about working on this topic from a variety of different vantage points. One of the more comprehensive studies on wakes in general, was done in [17]. It is a detailed description of the current understanding regarding the near and far wake. Others have taken a numerical approach, such as [18] and [19]. They used CFD to analyze the wake

effects. There have also been many experimental approaches to this topic as well. However, few experiments have used water as its working fluid. Among the ones that have are [20] and [21]. Though the rigs these researchers used were quite different from that used in this thesis. The reason using water can yield interesting and better results in some ways, will be discussed in section 3.2.

It is also worth noting that that this thesis is in many ways a continuation of the work done by former student at NTNU, Jenny Bjørnsgaard [22]. Also, some parts of this thesis is taken from my own project thesis done in the fall of 2016, on a similar topic.

1.4 Problem Formulation

An experimental facility has recently been installed at the NTNU Fluid Mechanics lab. This facility is a tow tank that can be used to conduct wind turbine experiments in water. The work on this thesis has been the first experimental work performed at the new facility. Performing experimental work on a new facility like this has meant dealing with many issues along the way. While the overall goal of the facility is conducting experiments on the near wake region of wind turbines (tip vortices more specifically), the purpose of this thesis has been to assess the performance the rig, and work out many of the issues that arise in a new facility. Testing the rig will allow for a better understanding regarding potential uses, as well as make future measurements better, and thus allow for a better understanding of the physics involved in future research projects. In order for the apparatus to be tested accurately, a series of experiments needed to be conducted, allowing for the overall aim to be broken down to the following three objectives:

- Creating a LabVIEW program that can accurately control the stepper motors. This includes being able to precisely set the traversing and rotational velocity, as well as a number of safety features. The program should be usable for others who are not familiar with it.
- Conduct an experiment reconstructing the trajectory of the blade, and finding information regarding the blade vibration. This includes work with camera calibration.

- Conduct preliminary flow visualization experiment, by injecting dye into the flow near the tip of the blade and visualizing tip vortices.

The blade tracking experiment is important because it allows for an assessment of whether or not the blade moves in a way that is similar to what a real life turbine would. That fact that the motion is similar to real turbines, is essential if one wants to apply the results on an industrial scale. The flow visualization experiment is important, because it allows one to uncover interesting physical properties of the wake.

1.5 Structure of Thesis

This thesis is structured as a technical report. Chapter 2 will focus on the theoretical background. This includes general theory on wind turbines and wind turbine wakes and more specifically the theory of the development of the near wake, including tip vortices. Chapter 2 will also include some information regarding camera calibration and flow visualization. These are all topics needed to be able to accomplish the objectives set out in 1.4.

Chapter 3 will focus on the methodology used to perform the various experiments. Each component of the rig will be explained in detail, dimensions and specifications. This includes the stepper motors, the blade, the tank, the calibration plate and the cameras used throughout the project. A step-by-step description of how each experiment was performed will also be in this chapter. This includes a description of the dye visualization experiment, as well as the blade tracking experiment.

Chapter 4 will present the results of each of the experiments. First, the results from the flow visualization experiment will be shown, followed by a discussion regarding the results. Next will be a presentation of the results from the blade tracking experiment. Chapter 5 will, for the most part, be dedicated to a conclusion. Other than a conclusion, there will also be some ideas for possible further work that can be done to improve the rig.

Chapter 2

Literary Study

The purpose of this chapter is to give the reader an overview of the current state of research regarding wind turbine wakes. In section 2.1, there will be a brief introduction into the theoretical background of modern wind turbine design. Both actuator disc theory and blade element moment will be discussed, as well as their relation to the wake recovery. In section 2.2, there will be a theoretical overview of wind turbine wakes. Section 2.3 will delve more into detail regarding a specific part of wind turbine wakes, namely the tip vortices. There will be a description of how this phenomenon affects power output and loads on a wind turbine. Section 2.4 will give an overview of common ways to mitigate the wake losses, while section 2.5 will give a description of typical flow visualization methods. Finally, in section 2.7, there will be a brief theoretical background into the calibration techniques used in this thesis.

2.1 Fundamental Principles in Wind Turbine Design

2.1.1 Actuator Disc Theory

Consider an infinitely thin disc placed in incompressible flow as depicted in fig. 2.1. The disc is a device intended to extract energy from the wind. Since the disc will extract some percentage of the energy in the wind, the downstream velocity v_2 must be lower than the upstream velocity

v_1 due to mass conservation. The difference between these two velocities can be described by the *axial induction factor* a . This factor represents the velocity lost in the actuator disc.

$$a = \frac{v_1 - v}{v_1} \quad (2.1)$$

From (2.1) it can be shown that:

$$v = v_1(1 - a) \quad (2.2)$$

$$v_2 = v_1(1 - 2a) \quad (2.3)$$

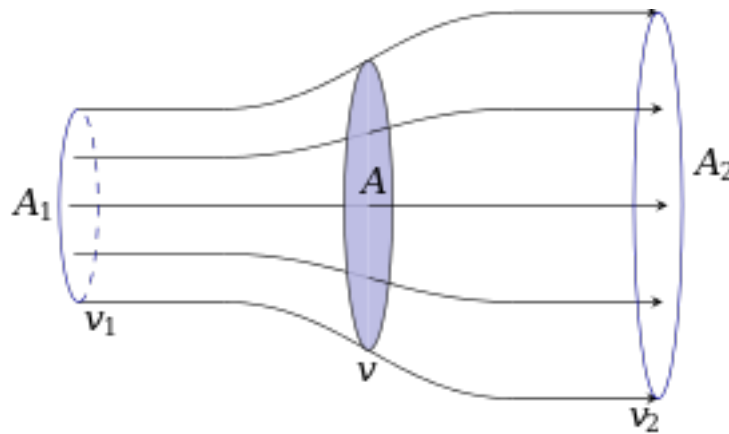


Figure 2.1: Actuator Disc [3]

A weakness of this theory is the incompressible flow assumption. Near the tip of the blade, one might obtain velocities upwards of $100 \frac{\text{m}}{\text{s}}$ [23], which should be considered compressible flow.

The reason this subject is relevant to this thesis, is because of the correlation between the energy extracted and the velocity deficit in the wake recovery. The actuator disc theory was developed in order to obtain knowledge regarding simple systems with only a single turbine (or propeller for that matter) [24]. Actuator disc theory does not take into account the effects that might occur downstream of the actuator disc.

2.1.2 Blade Element Momentum Theory

When designing a turbine blade used for wind turbines, the blade element momentum theory (BEM) is commonly used. It is useful in order to derive equations for determining the torque and thrust on a wind turbine blade. In this method, one divides the turbine blade into N elements. The main assumptions made here are [25]:

- Each element can be treated individually from one another, meaning that there is no interaction between the blade elements.
- The only forces on the blade elements are determined by the lift and drag coefficients.

However, the blade elements will experience different conditions, due to the fact that there are different chord lengths c , rotational speed Ωr and twist angle ϕ . In fig. 2.3 one can see the the forces dF_L and dF_d acting on a blade element.

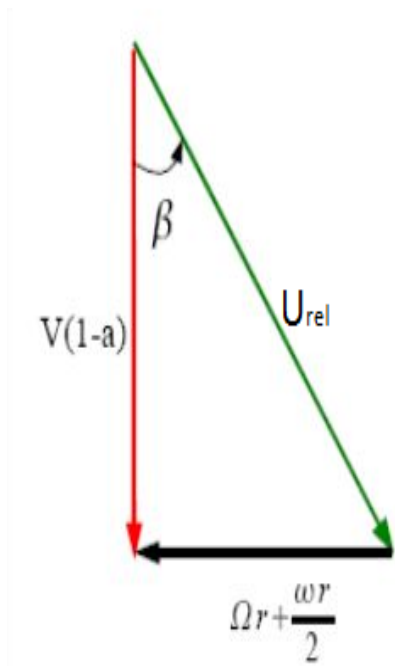


Figure 2.2: Relative velocity [4]

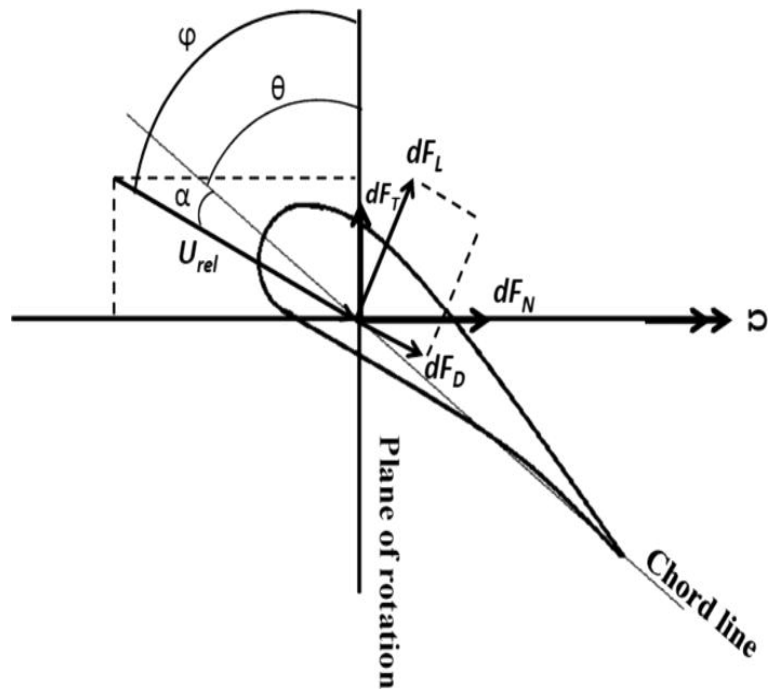


Figure 2.3: Forces Acting on an Airfoil [5]

Where dF_T and dF_D are the forces acting in the axial and tangential direction on the blade element. dF_L and dF_d are the lift and drag forces acting on an element. α is the angle of attack. U_{rel} is the relative velocity. θ is known as the *pitch angle*, it is the angle between the chord line

and the rotor plane. ϕ is the angle between the flow direction and the rotor plane.

In the same way the axial induction factor a was defined in section 2.1.1, the angular induction factor a' can be defined:

$$a' = \frac{\omega}{2\Omega} \quad (2.4)$$

Where ω is the angular velocity of the flow leaving the blade. While Ω is the angular velocity of the blades themselves. Using (2.4) and fig. 2.2 one can obtain expressions for the angle β based on the induction factors as well as relative velocity U_{rel} :

$$\tan(\beta) = \frac{r\Omega(1+a')}{v(1-a)} \quad (2.5)$$

$$U_{rel} = \frac{r\Omega(1+a')}{\sin(\beta)} = \frac{v(1-a)}{\cos(\beta)} \quad (2.6)$$

By considering the forces acting on each blade element seen in fig. 2.3, expressions for the forces in the angular and tangential direction can be obtained:

$$dF_T = dF_L \cos(\beta) - dF_d \sin(\beta) \quad (2.7)$$

$$dF_n = dF_L \sin(\beta) - dF_d \cos(\beta) \quad (2.8)$$

Where β is the angle between the direction of the tangential force and the direction of the lift.

Determining dF_L and dF_d , can be done by using the definition of the lift and drag coefficients:

$$dF_L = \frac{1}{2} C_L \rho U_{rel}^2 c dr \quad (2.9)$$

$$dF_d = \frac{1}{2} C_d \rho U_{rel}^2 c dr \quad (2.10)$$

combining (2.7) and (2.8) with (2.9) and (2.1.2) yields the following expression for the forces acting in the tangential and axial direction:

$$dF_T = \frac{1}{2} \rho U_{rel}^2 (C_L \cos(\beta) - C_d \sin(\beta)) B \quad (2.11)$$

$$dF_n = \frac{1}{2} \rho U_{rel}^2 (C_L \cos(\beta) + C_d \sin(\beta)) B \quad (2.12)$$

Where B is the number of turbine blades. from this we find the torque by simply multiplying the tangential force by the radius at a given blade element r , yielding:

$$dT = \frac{1}{2} \rho U_{rel}^2 (C_L \cos(\beta) - C_d \sin(\beta)) Br \quad (2.13)$$

The torque is what "drives" the turbine. One can clearly see that the torque is negatively affected by drag and positively affected by lift. It is therefore desirable to design a blade that produces the highest lift to drag ratio possible. The thrust on the other hand, can be seen to have a negative impact on the structural integrity of the turbine. The thrust force needs to be supported by the foundations of the turbine in order to not tip over. The thrust, as we can observe from (2.12) has positive contributions from both the lift and the drag forces. Using the equations developed for the thrust and torque on a blade element, one can use an iterative scheme in order to obtain values for an optimal chord length c or tip speed ratio λ . For more details on this iterative process, see [26].

Considering the fact that the blade element momentum method is widely used for turbine blade design. It is important to understand its limitations. BEM does not at all account for wake effects. This is an apparent weakness, considering virtually all new wind turbines are placed in wind farms along with other turbines. As will be described in section 2.4, what is optimal turbine design for a single turbine, might not be the design that creates the optimum wind farm efficiency. This is particularly the case for the tip speed ratio λ [27]. Ideally, one would hope to be able to incorporate wake effects into BEM at some point, in order to be able to optimize efficiency for the wind farm at large.

However, there are methods of evaluating the wake recovery. Usually, these methods distinguish

between near and far wake (see section 2.2 for distinction between the near and far wake). For the near wake, common methods are the asymptotic acceleration potential method [28] and the the lifting-line free vortex wake method [29]. For the far wake, one typically uses kinematic models and field models [17]. Since this project will be considering the near wake, it would be quite interesting to validate the results of future experiments against the lifting-line free vortex wake method.

2.2 Wakes

In General, a wake is a region of velocity deficit due to energy extraction. In order for a wake to form, the body needs to experience a drag force. This drag results in a loss of momentum, causing a region (wake) with reduced velocity. The region in which the wind velocity increases from this reduced velocity, to that of the original free-stream velocity, is known as the wake recovery region. Bodies that have a streamlined shape are more affected by viscous drag, while blunt objects are more affected by pressure drag. The characteristics of the wake are mostly determined by two main factors, the shape of the body and the Reynolds number of the flow [30]. For blunt bodies, the wake is more affected by pressure drag, while for streamlined objects, frictional drag is more influential [30].

When considering the aerodynamic properties of airfoils, both cases (frictional drag dominated wakes, and pressure drag dominated wakes) will occur. For small angles of attack, the body can be considered streamlined, while when the angle of attack approaches stall (10-14°), the airfoil behaves more like a blunt object.

2.2.1 Wake Effects

The wake recovery can be highly influential in determining the total output in a wind farm [31]. It can also be important in determining loads on downstream turbines in a wind farm array system. The reason for this, is simply the decreased amount of energy in the wind, due to a lower mean velocity of the flow field in the wake of a turbine, as well as increased turbulence

levels.

The negative impact of the wake on downstream turbines, is a more prominent feature in off-shore wind farms, as opposed to onshore. This is because of lower atmospheric turbulence onshore as opposed to offshore. This means that the wake of offshore wind farms will persist for longer [32]. Given that much of future wind power installations are likely to be offshore, the importance of this topic is set to only increase in the future.

2.2.2 Wake Structure

The wake of a rotating wind turbine is typically divided into two separate regions with different flow characteristics. The near wake and the far wake.

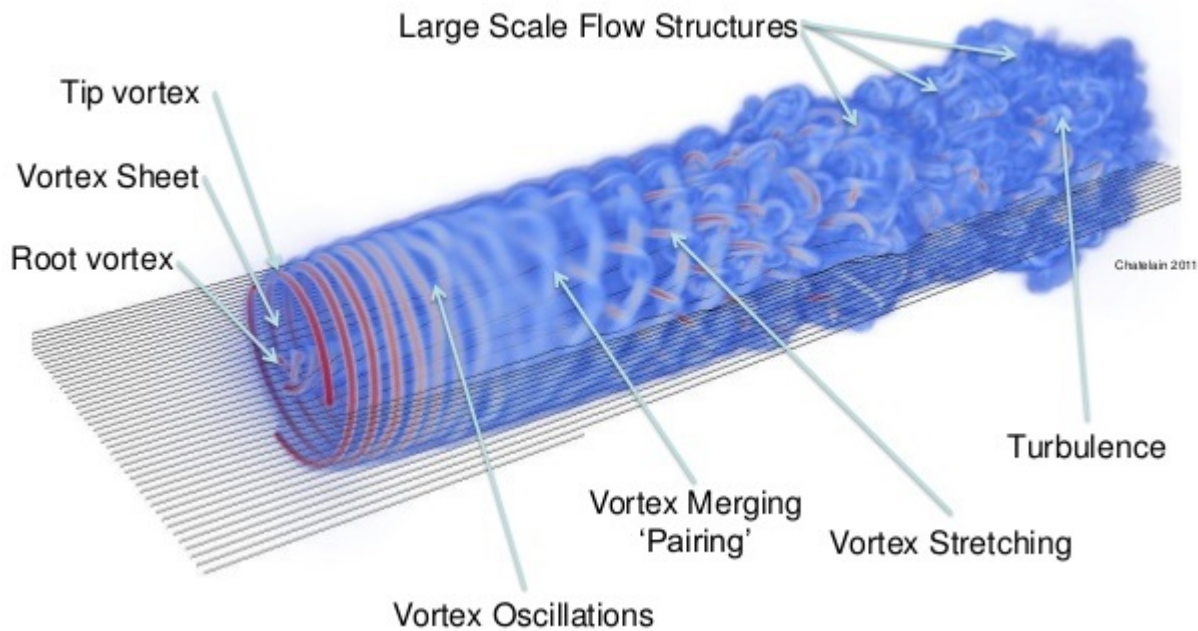


Figure 2.4: Wake development broken down into sections [6]

The near wake is the region immediately behind the turbine, up to about one rotor diameter downstream. In this region, the shape of the rotor has a significant impact. One may also experience significant 3D effects, as well as tip- and hub vortices in this region [17]. The area where tip vortices "merge", marks the transition between near and far wake. This usually occurs when the tip vortices begin to "leapfrog" one another before eventually becoming turbulent flow struc-

tures in the far wake. In the region of the wake where the leapfrogging occurs, there is a sudden increase in turbulent mixing [27].

The far wake is the region beyond the near wake, and before the next turbine in the array. The next turbine can be anywhere from 3 to 10 diameters downstream depending on specific site specification [33]. In this region, the shape of the turbine blade is less important. Other factors such as atmospheric effects, turbulence and velocity deficit (wake models) are more important. This region is dominated by large-scale flow structures and turbulence. It is in this region that other turbines are placed in a typical wind farm array system. Even though the near and far wake have distinctly different characteristics, there is a clear correlation between the two regions. The degree to which the vortex breakdown is occurring in the near wake has a clear impact on the aerodynamic properties of the far wake, and thus the power output of the downstream turbines [34].

2.3 Tip Vortices

Tip vortices are a flow phenomenon occurring in the near wake region, as mentioned in section 2.2.2. Tip vortices occur due to pressure differences between pressure and suction sides of the turbine blade [35]. This causes what is known as vortex shedding. The fact that the vortex pathlines take a helical shape simply has to do with the fact that the turbine blades are rotating.



Figure 2.5: Tip vortices visualized using smoke [7]

This same physical phenomenon also occurs at the turbine hub, resulting in a hub vortex. These vortices are not nearly as strong as the tip vortices, and are much harder to visualize [35] [17].

2.4 Mitigating Losses

The end goal of this kind of research is to increase the power output of wind farms. Wake losses account for the largest decrease in efficiency for large scale wind farms [36]. An obvious way this could be mitigated is by simply increasing the distance between the turbines. However, available land is becoming more and more scarce as more wind farms are developed. Also, the public demand for preserved recreational areas, as well as nature conservation concerns, make this option not very viable.

Some research [8] seems to indicate that the tip speed ratio λ of the turbine might prove to be an influential factor in the strength. Thus, it also has a significant impact on the wind farm power output. This has to do with the way the tip speed ratio affects the effective angle of attack. Consider the definition of λ :

$$\lambda = \frac{\Omega R}{V_0}$$

This same relation is what defines the effective angle of attack. This can be seen in fig. 2.6.

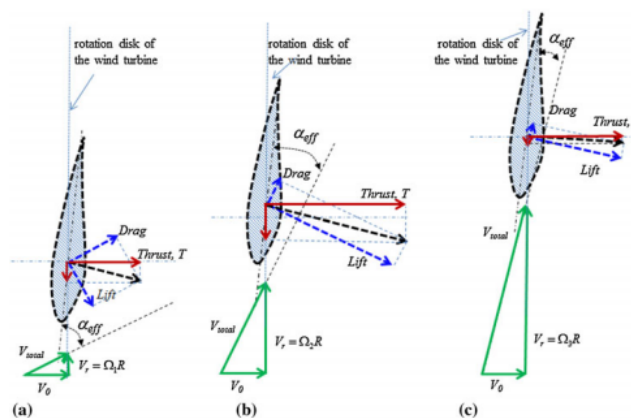


Figure 2.6: Effective angle of attack for varying tip-speed ratio [8]

Increasing λ decreases the effective angle of attack. Smaller angles of attack yield a less blunt and more streamlined body, as described in section 2.2. This means that there is less of a pressure difference across the blade, thus causing weaker tip vortices. Weaker tip vortices cause a quicker transition into the region where the tip vortices merge, yielding less of a distance needed to re-energize the wake. One must keep in mind that λ is a design parameter. Typically, a well-designed three bladed turbine has a value of about $\lambda = 6 - 7$. Increasing λ might have a negative impact on the efficiency of each individual turbine even though it decreases the wake losses. One must balance the desire to optimize each turbine, with the need to optimize the efficiency of the wind farm as a whole.

The notion that weakened tip vortices yield a quicker transition and vortex merging is discussed in detail in [8]. They found that the distance between neighbouring tip vortices would decrease almost linearly for increasing λ . The same was found in [27]. Once the vortices begin to merge, there is a drastic increase in turbulence production, causing the re-energizing of the wake to begin [27]. [27] also found that increased strength of the vortices caused added turbulence production.

Another factor that seems to be able to decrease the wake loss, is the wind turbine yaw. Yawing might be able to mitigate the losses somewhat [37]. Adjusting the yaw angle changes the trajectory of the near wake, yielding lower wake losses for the downstream turbines. However, atmospheric conditions seem to have a larger impact than the yaw angle.

2.5 Flow Visualization

Flow visualization using dye and smoke are some of the oldest methods on record [38]. Many groundbreaking discoveries have been made using these methods, among these is the legendary experiment by Osborne Reynolds in 1883 (see fig. 2.7), showing the transition between laminar and turbulent pipe flow [39]. The main advantage of dye and smoke, is that they are both simple and cheap. Traditionally, flow visualization has been used to obtain qualitative information regarding the flow. However, in recent years, some flow visualization techniques, have been able to gather quantitative information. One of these techniques, is Particle Image Velocimetry

(PIV) [40].

Another way of uncovering flow patterns through flow visualization, is by using seeding particles, a light source and a camera (preferably a camera with high resolution and frame rate). The seeding particles should avoid effecting the flow. This can be done by ensuring the particles size, and weight is appropriate for a given experiment. The challenge is to not use so much seeding particles that they effect the flow patterns significantly, while still using enough to obtain good images.

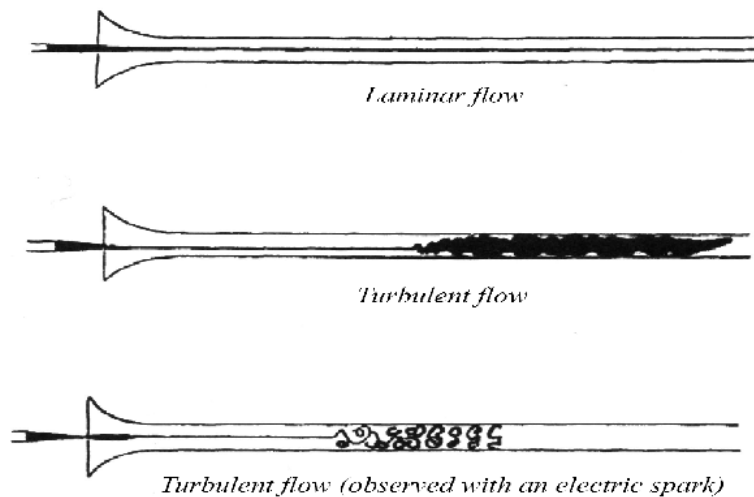


Figure 2.7: Osborne Reynolds' sketches of laminar to turbulent transition [9]

One of the advantages of performing the experiment using water is that it makes it easier to perform flow visualization for appropriate Reynolds number [41]. This feature is described in section 3.2.

2.6 Starting Vortices

Starting vortices are caused by a sudden acceleration of an airfoil from a position at rest [42]. These vortices are produced by the same type of pressure differences as cause the tip vortices as described in 2.2. The difference being that the starting vortices are broken down quickly due to viscosity effects, while the tip vortices are maintained over time while the turbine operates at a fixed rate.

2.7 Camera Calibration

In order to be able to perform the blade tracking experiment, accurate camera calibration became a necessity. Being able to map the pixel coordinates of an image to actual world coordinates is essential for obtaining quantitative 3D about the trajectory of the blade. The most common way of obtaining world coordinates from pixel coordinates is by using what is known as the pinhole model. However, in this thesis, a different approach has been used. In this thesis, the camera calibration is performed based on polynomial fitting, as described in section 2.7.2.

A challenge associated with camera calibration lies in the fact that the calibration is only valid for one particular setup. Changing the plane of observation or shifting the camera's position will necessitate additional calibration if one wishes to obtain accurate quantitative data. For the flow visualization of this project, the camera calibration was not as important. However, for the blade tracking experiment, calibration was essential.

2.7.1 Pinhole Model

The Pinhole Model is the simplest way of describing the triangulation between pixel coordinates and world coordinates. The model is illustrated in fig. 2.8. The key to this method is to use set the Z-coordinate of the 2D image to the optical axis of the camera and to fix the origin of the 2D image to the optical center of the lens.

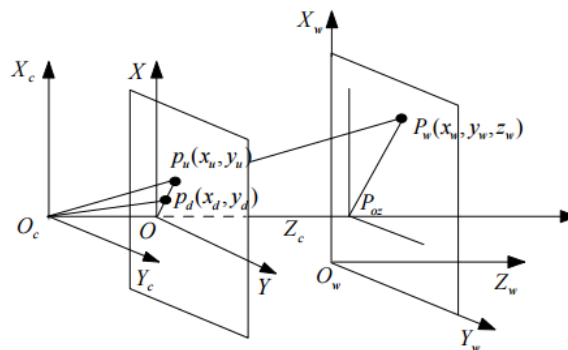


Figure 2.8: Important and interesting caption [10]

This model yields the following equation for the transformation between image coordinates and

world coordinates.

$$s \begin{bmatrix} u \\ v \\ 1 \end{bmatrix} = \begin{bmatrix} \frac{1}{d_x} & 0 & u_0 \\ 0 & \frac{1}{d_y} & v_0 \\ 0 & 0 & 1 \end{bmatrix} \begin{bmatrix} f & 0 & 0 & 0 \\ 0 & f & 0 & 0 \\ 0 & 0 & 1 & 0 \end{bmatrix} \begin{bmatrix} K & T \\ 0^T & 1 \end{bmatrix} \begin{bmatrix} x_w \\ y_w \\ z_w \\ 1 \end{bmatrix} = \begin{bmatrix} \alpha & 0 & u_0 & 0 \\ 0 & \beta & v_0 & 0 \\ 0 & 0 & 1 & 0 \end{bmatrix} \begin{bmatrix} K & T \\ 0^T & 1 \end{bmatrix} \begin{bmatrix} x_w \\ y_w \\ z_w \\ 1 \end{bmatrix} \quad (2.14)$$

Where the camera's intrinsic parameters are given by: α, β, u_0 and v_0 , while the camera's external parameters are given by K and T . So one can see, that this method necessitates knowledge of the camera's intrinsic and extrinsic parameters. u and v are the 2D pixel coordinates of the 2D image.

2.7.2 Camera Calibration Based on Polynomial Fitting

By utilizing a polynomial based calibration approach, one can avoid having to ascertain the specific camera parameters. To show this, one can start with equation 2.14. By using a minimum of 6 points, with known 3D coordinates, on two different z -planes, one can substitute the intrinsic and extrinsic parameters with a projection matrix M by using least square method [10]. This yields the following:

$$s \begin{bmatrix} x_w \\ y_w \\ z_w \\ 1 \end{bmatrix} = \begin{bmatrix} m_{11} & m_{12} & m_{13} & m_{14} \\ m_{21} & m_{22} & m_{23} & m_{24} \\ m_{31} & m_{32} & m_{33} & m_{34} \end{bmatrix} \begin{bmatrix} x_w \\ y_w \\ z_w \\ 1 \end{bmatrix} \quad (2.15)$$

Writing this out yields:

$$(m_{11} - um_{31})X_w + (m_{12} - um_{32})Y_w + (m_{13} - um_{33}Z_w) = um_{34} - m_{14} \quad (2.16)$$

$$(m_{21} - vm_{31})X_w + (m_{22} - vm_{32})Y_w + (m_{23} - vm_{33}Z_w) = vm_{34} - m_{24} \quad (2.17)$$

Thus, by obtaining the coordinates of a point on the 2D image, one can move on to obtaining the 3D world coordinates.

Chapter 3

Methodology

In this chapter, the methodology of the experiments conducted in this thesis will be explained in detail. First, an experimental motivation will be given. The motivation for conducting experiments in the blade tow tank in general, as well as for each of the two specific experiments will be described. Next, there will be a detailed portrayal of all the components of the blade tow tank rig. This includes the tank itself, the blade, the camera, the stepper motors and the LabVIEW program used to control them. In section 3.2, there will be a description of the possibilities yielded by dynamic similarity considerations due to the use of water as opposed to air as the working fluid.

Finally in this chapter, will be a description of each of the two experiments. First the blade tracking experiment, followed by the flow visualization experiment. This description will include information regarding the approach and setup of the experiments, as well as equipment and components specific for each of the experiment. For the blade tracking experiments, this includes the calibration plate, while for the blade tracking experiment, it includes the dye injection setup.

3.1 Experimental Motivation

As laid out in section 1.4, performing actual experiments, is the only way to sufficiently test the blade tow tank rig. This is the main motivation for the experiments conducted in this thesis. Two experiments were performed. The first was to analyze the degree to which the blade vibrated. The other was to attempt to visualize tip vortices.

For the blade vibration experiment, the motivation is closely linked to the overall aim of the thesis of testing the rig. If the blade vibrates more than a negligible amount, it will have detrimental effects on the wake properties, by introducing an unnatural movement in the blade. This will cause the wake to perform differently than one would expect on an actual wind farm, thus causing unreliable results in future wake experiments. Quantifying the blade vibration, as well as uncovering potential solutions, would be important for future work.

The motivation for the flow visualization experiment on the other hand, is to better understand physics of wind turbine wakes. More specifically, the tip vortices in the near wake. Performing flow visualization allows one to qualitatively assess the flow structure. The fact that the experiments are done in water can also be advantageous, as described in section 3.2. The flow visualization experiment is also linked to the overall aim of testing the facility, as the goal of the facility is to perform these types of experiments (among others). Thus, conducting the flow visualization experiment, would go further in assessing the rig.

3.2 Dynamic Similarity

The main advantage of working with water as the working fluid, as opposed to air, is that it allows for lower velocities at similar Reynolds number. To understand this point, a comparison to a study done in a wind tunnel has been made [43]. [43] is a blind study on wake effects. The study has used turbine blades with the NREL S826 airfoil. The model Reynolds number is $Re_{C,tip,model} = 10^5$, a tip speed ratio $\lambda = 6$ and an inflow velocity of $6 \frac{\text{m}}{\text{s}}$. There were used two different rotors in the study, one with a diameter of $D_1 = 0.9544 \text{ m}$ and $D_2 = 0.894 \text{ m}$. For the purpose of this comparison, the diameter D_1 will be used.

Water has a kinematic viscosity of $\nu_W = 1.004 * 10^{-6}$ at a temperature of 20 °C, while air has a kinematic viscosity $\nu_{Air} = 1.568 * 10^{-5}$. Meaning that the ratio between the two is $\frac{\nu_{Air}}{\nu_W} = 15.68$. This means that with similar geometries, one can reduce the inlet velocity and the rotational speed by a factor of 15.68. Considering the definition of the Reynolds number of $Re = \frac{vD}{\nu}$, this would yield an inlet velocity (translating into the traversing speed for this experiment) of $6 \frac{m}{s} * \frac{1}{15.68} = 0.382 \frac{m}{s}$, while still remaining dynamically similar with a Reynolds number of 10^5 . The rotational speed could also be greatly reduced from $\omega = 80 \frac{rad}{s}$ to $\omega = 5.10 \frac{rad}{s}$.

This has practical implications for this experiment. The reason being that one of the primary goals is to observe the tip vortices. For lower velocities, higher temporal resolution can be obtained, because the frame rate can be reduced. This yields better imagery for the region of the blade near the tip.

3.3 Blade Tow Tank Rig

The Blade Tow Tank Rig, is an experimental facility in the Fluid Mechanics Laboratory at NTNU. The rig consists of a tank, two stepper motors, a shaft and blade connected to the bottom of the shaft. In fact, there are two shafts, one inner shaft, connected to the blade, and one outer shaft holding the inner shaft in place. At the bottom of the tank there is also a spring, meant to minimize the impact of the blade potentially falling to the ground.

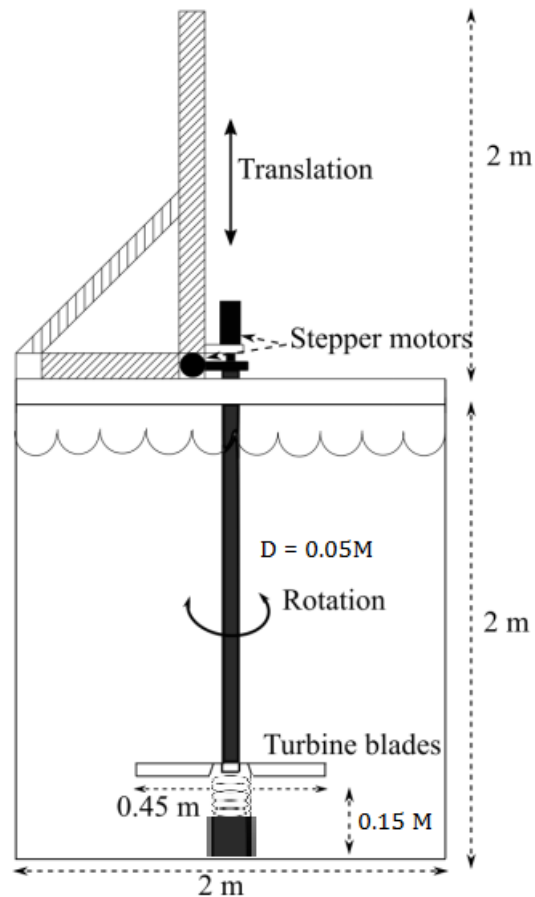


Figure 3.1: Blade Tow Tank Rig Schematic

There are many potential uses for the rig. Although this thesis is focused on applications associated with wind turbines, there is no reason why experimental work regarding for instance helicopter aerodynamics or shipping propellers could not be done here.

3.3.1 The Tank

The Tank used in this experiment is 12-sided, approximating a cylindrical shape. It has a height of 2 meters and a diameter of 2 meters. See to fig. 3.1 for a schematic description, or fig. 3.2 depiction of the tank.



Figure 3.2: Empty Tank

3.3.2 Stepper Motors

In order to traverse the blade up and down in the tank, as well as rotate it, two stepper motors were used. One stepper motor controlled the up and down motion of the blade, while the other handled the rotation of the blade. A stepper motor is a DC electric motor. It works by converting a series of input voltages (see section 3.4, for a description of how these voltages are generated), to a slight change in the position of the shaft. By controlling the position of the shaft, one can control the rotating, and traversing motion of the blade in this experiment. For a detailed description of how stepper motors operate, see [44]

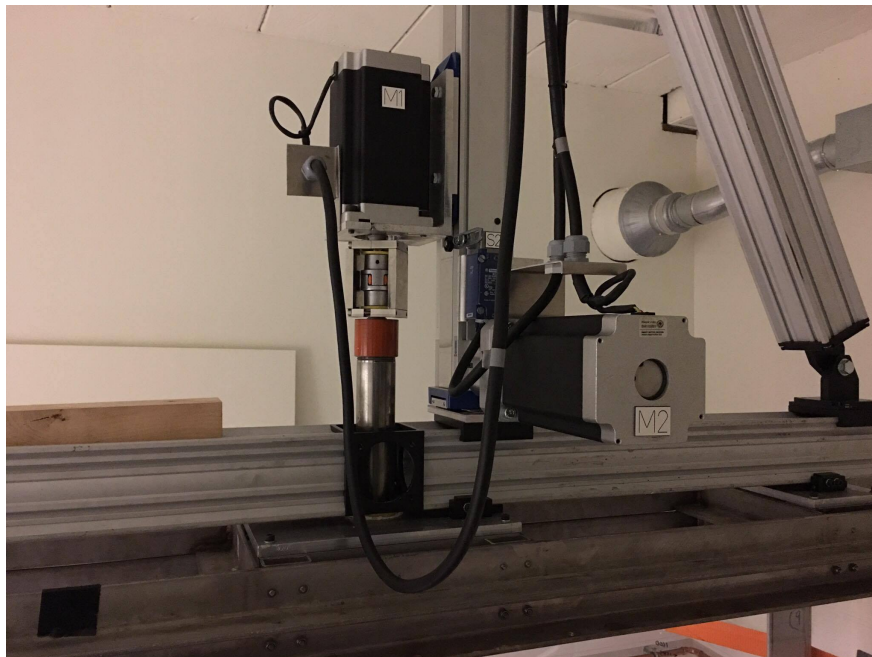


Figure 3.3: Stepper Motors

These stepper motors were able to perform so-called "micro-stepping", meaning that the motors can perform some 256 steps per 1.8 degrees of rotation. This yields a resolution of 51200 steps per rotation, which was sufficient for this experiment. The fact that stepper motors (with micro-stepping capabilities) can achieve such a high degree of precision makes them ideal for this kind of work[45]. By using micro-stepping, one can obtain a motion that is both easy to control and essentially continuous. The Stepper motors also were able to handle fast acceleration, allowing the blade to reach the intended rotational and traversing velocity quickly.

3.3.3 The Blade

The blade used for this experiment had a rectangular shape and the following dimensions:

- Length = 250mm
- Chord = 40mm
- Thickness = 2mm

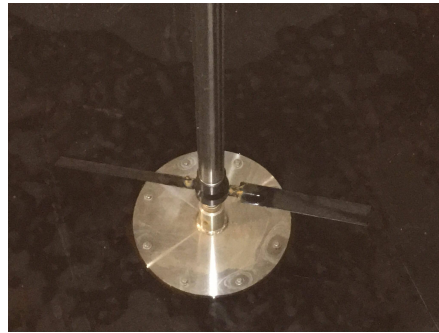


Figure 3.4: The Blade

The shape of the blade is far from what is used in normal horizontal axis wind turbines. Which makes the experiment less realistic. However, it is sufficient for some initial experiments.

3.3.4 The Camera

The camera used in this thesis is an IMPERX B4820 CCD camera. This is a high-speed progressive scan camera [46]. The camera has 16 megapixels, a frame rate of 3.2 frames per second and a maximum resolution of 4904 x 3280. The camera is not a part of the rig itself, but played an essential part to both experiments conducted in this thesis.



Figure 3.5: Wake development broken down into sections

3.4 Labview Script

During this project, I developed a LabVIEW program in order to enable accurate control of the stepper motors. This was done by using the LabVIEW software from National Instruments (NI) [47]. The purpose of this program is to generate digital signals. These signals are used to drive the stepper motors. As explained in section 3.3.2, the stepper motor translates a digital pulse into rotational or traversing motion of the blade by incrementing shafts position. The challenge faced in this project was controlling the generation of pulses accurately. Below is a flow chart describing how the program functions.

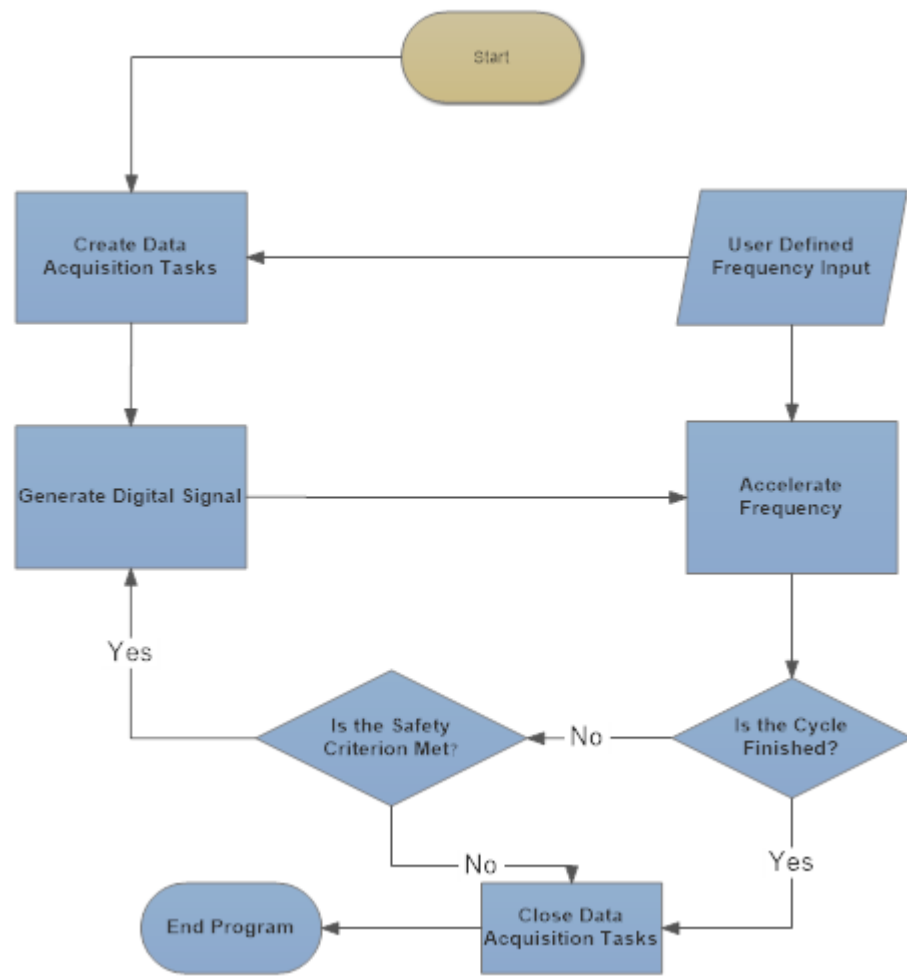


Figure 3.6: LabVIEW Flow Chart

An important feature with the code was its ability to accelerate the speed of the shafts traversing and rotational motion. This can be done by controlling the frequency at which the pulses are

generated. Without the ability to accelerate the frequency, the motors would be going from a standstill position to the desired velocity in virtually no time. This could potentially harm the blade.

The program is implemented in a way so that the user maintains control of the rotational and traversing velocity of the motors, as well as the rate of acceleration. This is done in what is known as the "Front Panel" of the program. This is where the user inputs all the relevant variables. In fig. 3.6, one can see the block that says "User Defined Frequency Input". This is where the parameters inputted by the user enters the code.

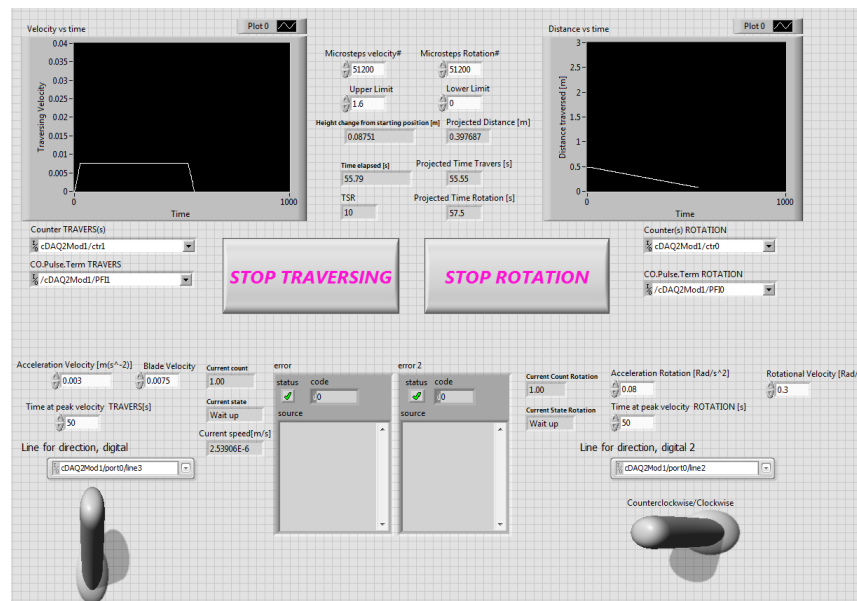


Figure 3.7: LabVIEW Front Panel

For the program to finish (without interaction by the user), one of two conditions must be met. Either the cycle must have finished, meaning that the blade reached its maximum velocity (decided by the user), maintained its maximum speed for a predetermined number of seconds before finally returning to a standstill position. Or, one of the safety criteria is violated. This occurs if the blade traverses past a predetermined upper or lower limit. This was implemented in order to ensure that the blade never crashes into the bottom or top of the tank. The programs also contain some graphical tools, that help the user determine the current position of the blade, as well as the current rotational and traversing velocity.

Finally, before the program begins to run, it outputs a series of important variables to the screen. These variables are the projected distance the blade will travel, the projected time it will use, as well as the tip-speed-ratio. This is done, to ensure the user has inputted the correct velocities. After these variables are outputted, the user is given a choice of running the experiment, or canceling.

3.5 Blade Vibrations Experiment

After running the experiment a number of times, it became apparent that the blades were vibrating somewhat. This was causing a disturbance in the flow, yielding less accurate flow visualization. In order to accurately quantify the effect of this vibration, an analysis was performed of the vibrations in the blade. Since this endeavour is more quantitative in nature, accurate camera calibration was a necessity. The theoretical background of the calibration performed in this experiment is described in section 2.7. The goal of the experiment was to accurately quantify the degree to which the blades vibrated. The reason the blades are vibrating might be due to a mechanical issue with the rig. One possibility is that there is a substantial amount of friction between the inner and outer shafts on the rig. The vibrations can be seen with the naked eye, by anyone running an experiment in with the rig. This possibility is supported by the fact that the vibrations are most prevalent when the blade traverses, instead of just rotating. When the blade traverses, is also when there is the most friction between the shafts.

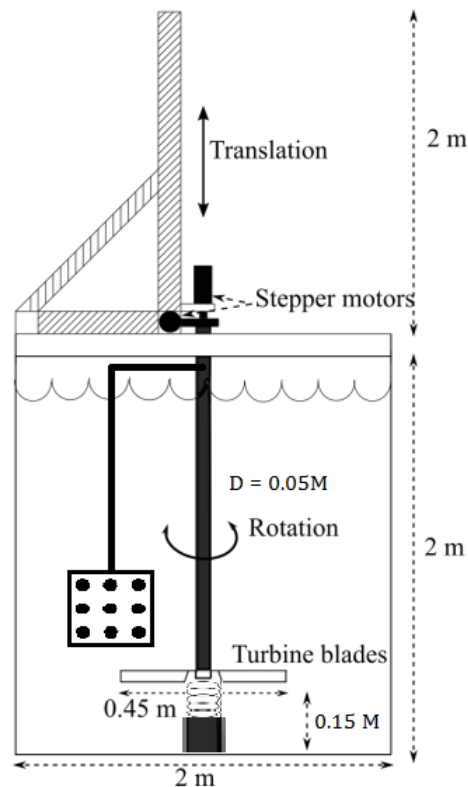


Figure 3.8: Calibration plate in tank

3.5.1 Calibration Setup/ Plate

The calibration plate used in this experiment, has the following dimensions:

- Area = 20X20cm
- Distance between dots = 15mm
- Distance between planes = 1mm

The plate is structured in an array of dots. The dots are placed on two different my-planes. This is done in order to facilitate polynomial camera calibration as explained in section 2.7.2. The pattern and distance of the dots are known, in order to be able to relate the pixel coordinates to world coordinates. The image of the calibration plate is taken while submerged in water, to make sure conditions are comparable to the actual experiment.



Figure 3.9: Calibration Plate

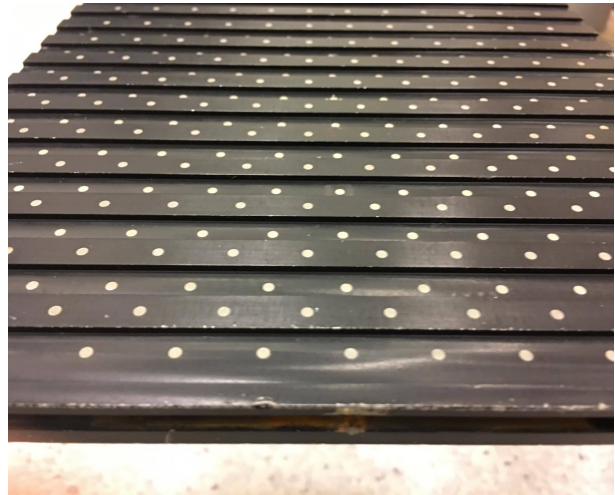


Figure 3.10: Calibration Plate tilted

A MATLAB script was used to obtain calibration data. The code can be viewed in section A of the appendix. After obtaining an image of the calibration plate, the user picks three calibration points on each XY-plane. From this, the MATLAB program is able to calculate data needed to convert the pixel coordinates to world coordinates.

3.5.2 Blade Tracking

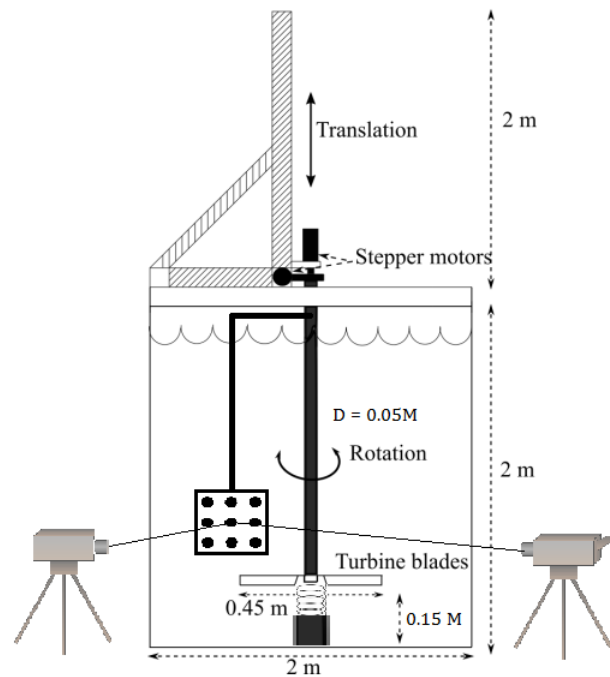


Figure 3.11: Line of sight of cameras intersecting at calibration plate

A white spot was painted on the blade, in order to have a specific, easily observable point to track, as seen in fig. 3.12. Two cameras are used, positioned about one meter apart, both focusing on the same point in the tank. The lines of sight of the cameras intersected at an angle of approximately 60 degrees, as depicted in fig 3.11. The reason for this was to be able to obtain a z-coordinate of the white dot. By finding the point, in 3D, at which the two lines of sight intersected, one can establish the z-coordinate. By doing this on a series of images, one obtains the trajectory of the blade. The z-coordinate, refers to the 3rd dimension in a Cartesian coordinate system.

The camera settings also played a significant role in obtaining good images. The camera's aperture setting, is what determines the *depth of field* [48]. Adjusting the aperture means adjusting the degree to which the camera lens is open to light. A smaller opening means less light, while a larger opening yields a larger depth of field. This is important, considering that the blade is moving throughout the frame. Inevitably, in some of the images, the blade will be out of focus,

simply because the depth of field was not large enough to cover the blade's movement throughout the frame. Less focus means less accurate determination of the dot's position in space.

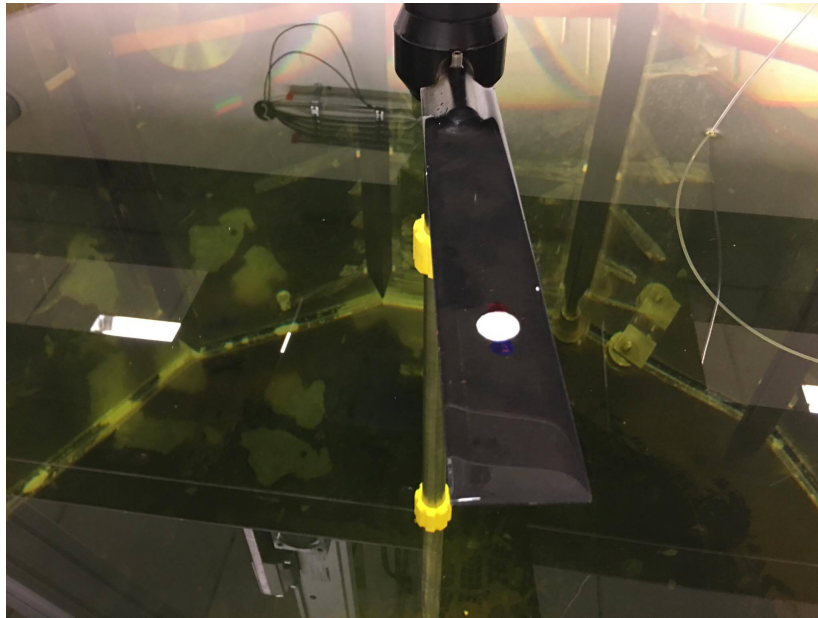


Figure 3.12: White dot on blade for blade tracking

The experiment can be broken down into the following steps:

1. Take an image of calibration plate, while the plate is submerged in water.
2. Calculate calibration data by choosing 3 points on each XY-plane of the calibration plate and running the MATLAB-script outlined in A.
3. Remove the calibration plate from the tank. Be careful not to move the cameras, as the calibration data is only valid for the exact position the cameras are in while the image of the calibration plate is taken
4. Rotate and traverse the blade in the tank. Make sure the white dot is visible for the cameras.
5. Take a series of images of the white dot, while the blade rotates and traverses in the tank.
6. Calculate the world coordinates of the white dot (and thus the blade), for each image.
7. Plot the blade's trajectory based on the obtained world coordinates

3.6 Flow Visualization Experiment

In order to visualize the flow in the wake of the blade, a rig had to be put in place in order to introduce the dye into the tank [49] [50]. Ideally one wishes to introduce the dye at a velocity similar to that of the flow in the region it is introduced, to avoid unnecessary disturbances in the flow. This velocity varies depending on the tip-speed-ratio used. For most of the experiments, the velocity will be around $0.03 \frac{\text{m}}{\text{s}}$. This means that the height of the container with the dye and the size of the tube needs to fit to yield this exit velocity. Another (more optimal) solution would be to use a pressurized container for the dye mixture. This would produce a more stable flow rate, that would not be dependent on the height of the water in the container. However, this was not available, so a gravity driven system was implemented.

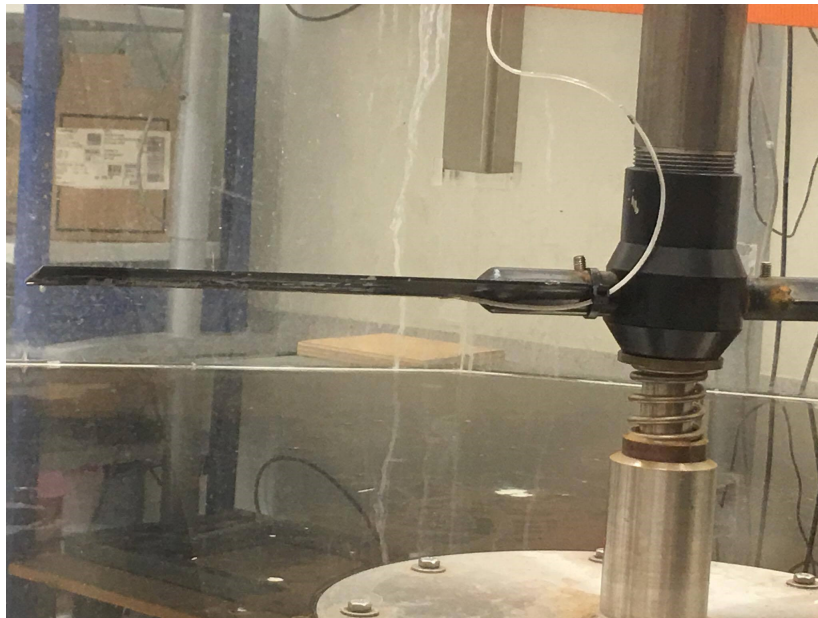


Figure 3.13: Tube used for dye injection

In order to keep the flow disturbance at a minimum, as thin a tube as possible was used. The chosen tube had an inner diameter of 1.5 mm. Smaller diameters were attempted, but the difficulty obtaining an adequate flow rate yielded the 1.5 mm option the obvious choice. The tube was positioned in such a way that the exit flow of the dye was parallel to the relative velocity of the flow. Since the relative velocity depends a great deal on λ , the tube needed to be repositioned for every new λ configuration. The way the tube was positioned, also forced the ex-

periment to be conducted using clockwise rotation (similar to what is used in industry), based on the systems frame of reference.

Other than dye, milk was also used in this experiment. Milk has several advantages over traditional dye solutions. Firstly, the contrast was better. This means that using milk yielded better imagery. Secondly, milk is produced with many different types of fat content. This means that finding the correct buoyancy can be found by simple trial and error. Finally, milk is easy to get a hold of and is relatively cheap. The biggest disadvantage using milk is that the tank and the tube need to be thoroughly rinsed after every experiment, in order to avoid bacteria growth. Since milk has a specific gravity that is slightly higher than water [51], water was added to the milk, in order to make it naturally buoyant.

The experiment can be broken down in to the following steps

1. Inject dye or milk into the flow near the tip of the blade.
2. Rotate the blade counterclockwise and traverse it upwards from a position near the bottom.
3. Take pictures of the tip vortices as they propagate throughout the tank.
4. Analyze the flow structure.

3.6.1 Calculating Flow Velocity

As mentioned in 3.6, the desired flow velocity is $0.03 \frac{\text{m}}{\text{s}}$ to correspond to the local flow velocity, while the desired pipe radius, is as small as possible, in order to minimize disturbances in the flow. Taking these two parameters into account while calculating the flow rate, a good place to start is the z-component of the Navier-Stokes equations (using cylindrical coordinates):

$$\rho \left(\frac{\partial u_z}{\partial t} + u_r \frac{\partial u_z}{\partial r} + \frac{u_\theta}{r} \frac{\partial u_z}{\partial \theta} + u_\theta + u_z \frac{\partial u_z}{\partial z} \right) = -\frac{\partial p}{\partial z} + \mu \left(\frac{1}{r} \frac{\partial}{\partial r} \left(r \frac{\partial u_z}{\partial r} \right) + \frac{1}{r^2} \frac{\partial^2 u_z}{\partial \theta^2} + \frac{\partial^2 u_z}{\partial z^2} \right) + \rho g_z \quad (3.1)$$

From equation 3.1 one can proceed to make the following assumptions:

1. Steady state conditions, meaning $\frac{\partial u_z}{\partial t} = 0$
2. velocity components in radial and axial directions are zero, $u_r = u_\theta = 0$
3. Fully developed and axis-symmetric flow, $\frac{\partial}{\partial \theta} = \frac{\partial u_z}{\partial z} = 0$

This yields the following:

$$\frac{1}{r} \frac{\partial}{\partial r} \left(r \frac{\partial u_z}{\partial r} \right) = \frac{1}{\mu} \frac{\partial p}{\partial z} + \rho g_z \quad (3.2)$$

Integrating with respect to r twice yields:

$$u_z(r) = r^2 \left(\frac{1}{\mu} \frac{\partial P}{\partial Z} + \rho g_z \right) + C_1 r + C_2 \quad (3.3)$$

Using the fact that the velocity needs to be non-zero at $r=0$ and the no-slip boundary condition of $u = 0$ at $r = R$, yields the following:

$$u_z(r) = \left(\frac{1}{\mu} \frac{\partial P}{\partial Z} + \rho g_z \right) (r^2 - R^2) \quad (3.4)$$

Finally, we assume that the pressure loss is constant throughout the pipe $\frac{\partial P}{\partial Z} = \frac{\Delta P}{L}$, and that the maximum velocity is at the centerline $r = 0$ (because of the parabolic shape of the velocity profile).

$$u_{z,max} = \left(\frac{1}{\mu} \frac{\Delta P}{L} + \rho g_z \right) R^2 \quad (3.5)$$

Knowing that the maximum velocity is double the average velocity for laminar flow, yields the following equation for the pressure loss throughout the pipe:

$$\Delta P = \frac{32\mu L u_{z,avg}}{D^2} \quad (3.6)$$

This pressure loss needs to be overcome, in order for the dye to exit the pipe at a non-zero velocity. Using the assumptions already made as well as considering flow along a streamline, one can obtain the Bernoulli equation. This can be used to calculating the exit velocity at different tube-lengths and diameters.

$$H_{in} - H_{out} = \Delta P g h = \frac{32\mu L u_{z,avg}}{D^2} \quad (3.7)$$

$$\left(\frac{v_2^2}{2g} + \frac{P_2}{\rho g} + h_2\right) - \left(\frac{v_1^2}{2g} + \frac{P_1}{\rho g} + h_1\right) = \frac{32\mu Lv_2}{D^2} \quad (3.8)$$

Assuming $v_1 = 0$, $h_2 = 0$ (reference height), $P_1 = 0$ (Open to atmosphere), $u_{z,avg} = v_2$, one can simplify equation 3.7 to:

$$\frac{v_2^2}{2g} + \frac{P_2}{\rho g} - h_1 = \frac{32\mu Lv_2}{D^2} \quad (3.9)$$

This equation can be solved for v_2 using different values for the parameters L and D. This has been done in a MATLAB script, that can be viewed in the appendix.

Chapter 4

Results

In this chapter, the focus will be on displaying the results of the flow visualization experiment. Imagery from both starting vortices and tip vortices will be displayed. The results of the quantitative analysis of the blade vibrations will also be presented in this chapter.

In order to obtain a clearer view of the vortices in the flow visualization experiment, some image processing has been done. Mainly, the constant background in the images has been subtracted, while the vortex contrast has been increased. The background was calculated by finding the average pixel intensity for a series of images. The contrast was increased by simply squaring all pixel intensities, so that the areas with tip vortices (Which have a higher intensity) are further enhanced. An example of this processing can be viewed in fig. 4.2 and fig. 4.1



Figure 4.1: Unprocessed Image

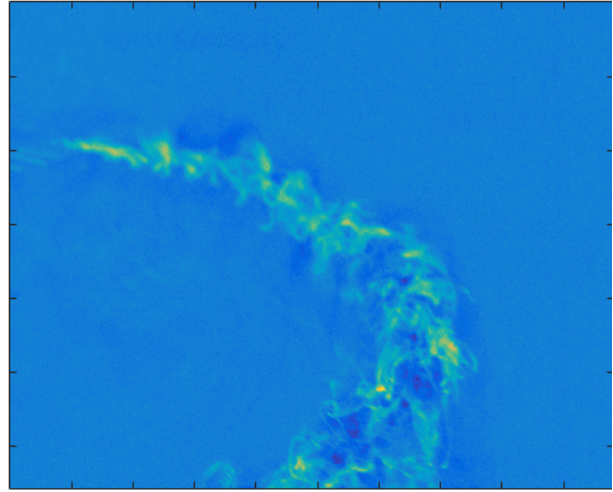


Figure 4.2: Processed Image

Each pixel value is represented by a color in a colormap. The image is set to use the full range of colors. Blue means that the pixel has a low value, while the yellow means the pixel has a high value.

4.1 Flow Visualization

The following results come from the experiments described in section 3.6.

4.1.1 Tip Vortices

In order to quantify the strength of the vortices, an analysis of the change in intensity between images was performed. This was done by selecting two images of the vortices directly after the blade had passed through the frame. The average of the difference between the images, was then divided by the average of the sum of the two images, to find the change between them in percentages. This can be described by the following equations:

$$ImageSum = Image2 + Image1$$

$$ImageDiff = Image2 - Image1$$

$$\%Change = 100 * (mean(ImageDiff)/mean(ImageSum))$$

The change in intensity between the images is an estimation of the vortices' strength. λ between 6 and 10 were used. This analysis yielded the following plot:

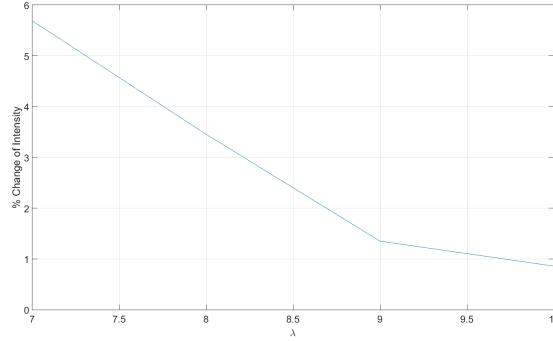


Figure 4.3: Strength of vortices

The following images show the visualization of tip vortices for λ between 6 and 10. For each λ , an aggregate of several images has been taken in order to obtain a visualization of the vortices as they progress over time. To calculate the aggregate, a series of images in sequence have been added together. First the background is removed, and contrast is added to each image in the sequence as is done for fig. 4.2. The next step is to simply add together all these processed images in order to reveal flow pattern that appears over time. The motivation for doing this, is to be able to observe the changes in flow structure over time, in only one image. This process can be described by the following equation:

$$AggregatedMotion = \sum_{t=1}^{tmax} Image(t) \quad (4.1)$$

Images of the change in intensity are also included. These are calculated by subtracting an image of the tip vortices by the previous image in that specific time sequence. By doing this, one can reveal changes in the vortices that occurred in the between when those two images were taken. This can be described by the following equation:

$$IntensityChange = Image(t) - Image(t - 1) \quad (4.2)$$

Where Image(t) is a processed image taken at the time t.

$\lambda = 6$:

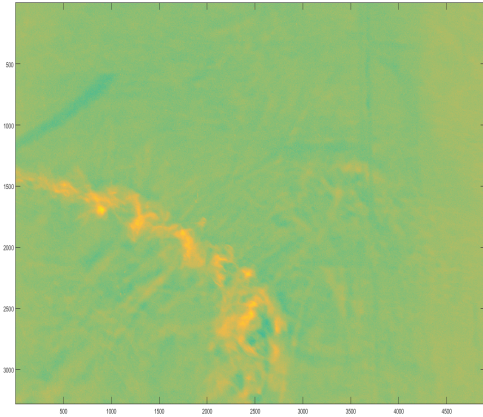


Figure 4.4: Aggregated Motion of tip Vortices

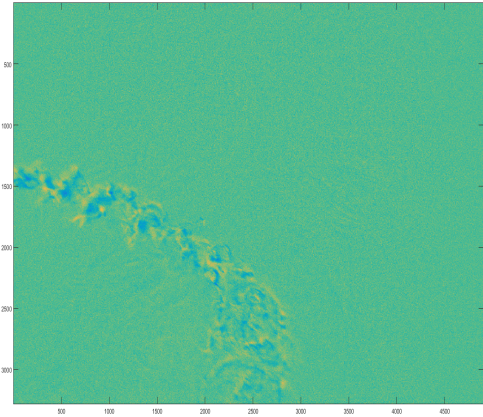


Figure 4.5: Intensity change between images

$\lambda = 7$:

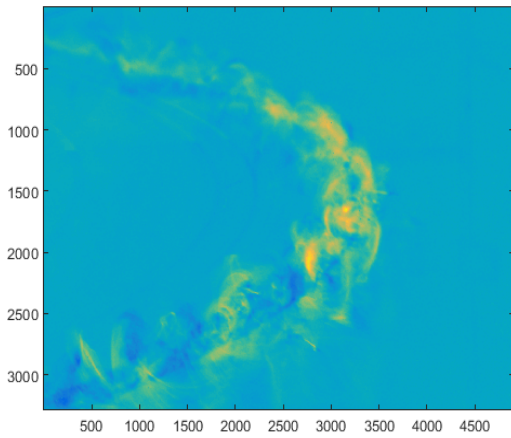


Figure 4.6: Aggregated Motion of tip Vortices

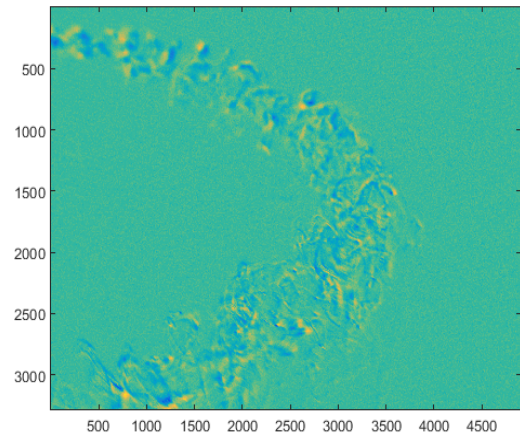


Figure 4.7: Intensity change between images

$\lambda = 8$:

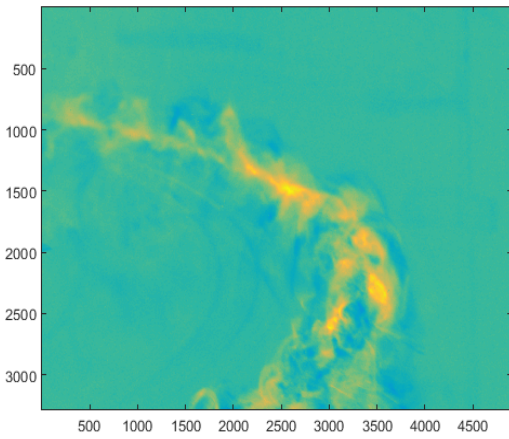


Figure 4.8: Aggregated Motion of tip Vortices

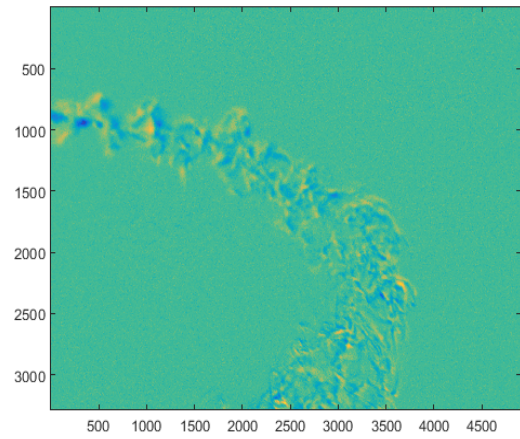


Figure 4.9: Intensity change between images

$\lambda = 9$:

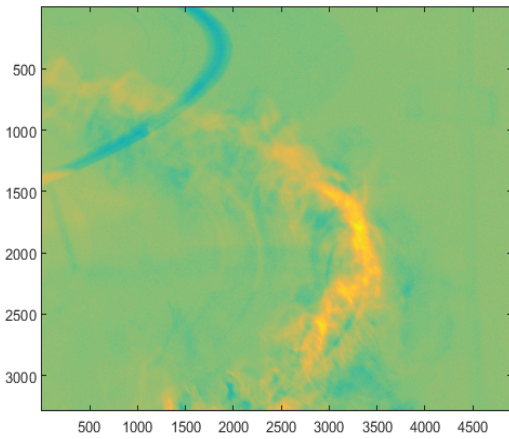


Figure 4.10: Aggregated Motion of tip Vortices

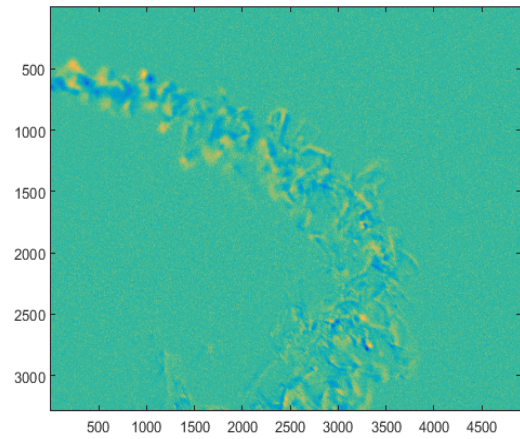


Figure 4.11: Intensity change between images

$\lambda = 10$:

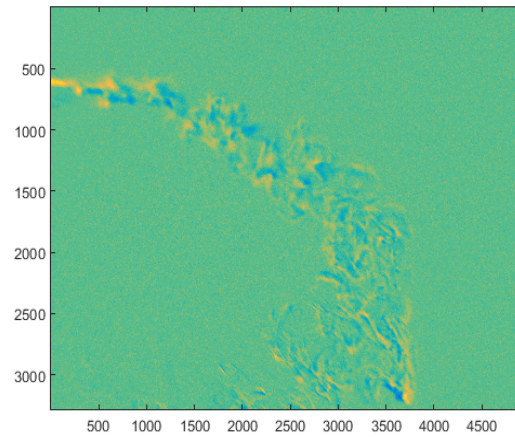
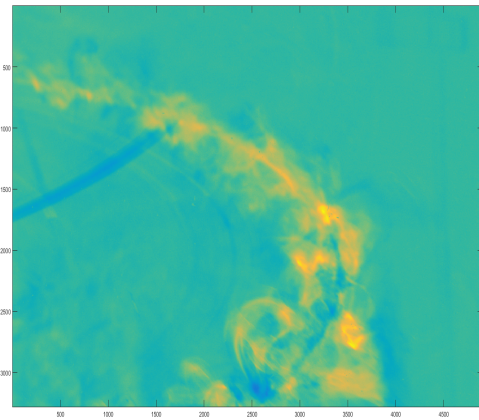


Figure 4.12: Aggregated Motion of tip Vortices Figure 4.13: Intensity change between images

4.1.2 Starting Vortices

A similar analysis as described in section 4.1.1 for the tip vortices, was performed for the starting vortices as well. The results are displayed in the images below.

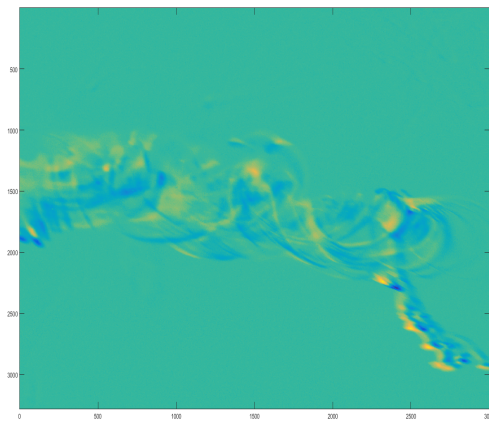
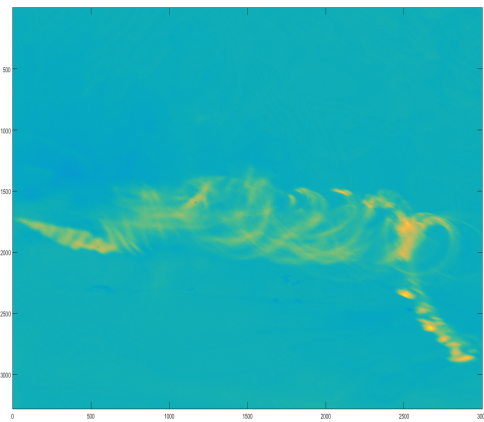


Figure 4.14: Starting vortices for $\lambda = 2.5$

Figure 4.15: Intensity change between images

4.2 Discussion Regarding Flow Visualization

Considering the problem formulation described in section 1.4, one can consider this experiment successful. The aim of this experiment was to Conduct preliminary flow visualization experiment, by injecting dye into the flow near the tip of the blade and visualizing tip vortices. Figures 4.4 - 4.12 show that this was indeed accomplished. The rig operated as intended, and visualization of the tip vortices was obtained. From a qualitative point of view, one can clearly see the tip vortices, as they propagate throughout the frame of the image. The starting vortices were even clearer in this visualization. Both the images of the aggregated motion the vortices, as well as the intensity change images yielded important qualitative information regarding the flow. More importantly, the images validated the rig itself, proving that vortex flow visualization is indeed possible using this setup.

Visualizing the vortices is a much easier task while viewing the images in a time series sequence. This allows for the viewer to observe the propagation of the vortices. Displaying the aggregated motion of the vortices along with the change in intensity between images, is an attempt to circumvent this problem.

As for the quantitative analysis of the strength of vortices, this proved an expected pattern as seen in fig. 4.3. The strength of the vortices, measured by the intensity change between images, seemed to decrease with increasing λ as predicted. This might be due to the fact that increasing λ , yields an increased effective angle of attack, as described in section 2.4.

4.2.1 Sources of error

A potential source of error in this experiment was the choice of images used in order to calculate the intensity change and thus the strength of the vortices. The images that where chosen, where those taken directly after the blade leaves the frame. However, some sampling of other images taken at different times in the progression of the blade throughout the tank, revealed sometimes significantly different change in intensity. This suggests that using the intensity change might not be the best way to calculate the strength of vortices.

Another potential error source could be the clarity of the water. Throughout time used to conduct this experiment, the water quality has been an issue. The color of the water is distinctly green, yielding difficulties in creating adequate contrast for imaging. Several attempts at filtering the water were done. This process had some success in making the water clearer. However, this remains a problem to this day. With clearer water, the images would undoubtedly be clearer, and thus the vortices easier to visualize.

4.3 Blade Vibrations Results

4.3.1 Path of Blade

The following plots display a part the path of the blade in the tank for λ between 5 and 10. The section of the path displayed is the section in which the white dot on the blade was visible in the frame of both cameras, thus making it possible to calculate the correct z-coordinate as described in section 3.5.2. The images were taken at a frame rate of 3.25 fps, which is also the maximum of what the camera was capable of.

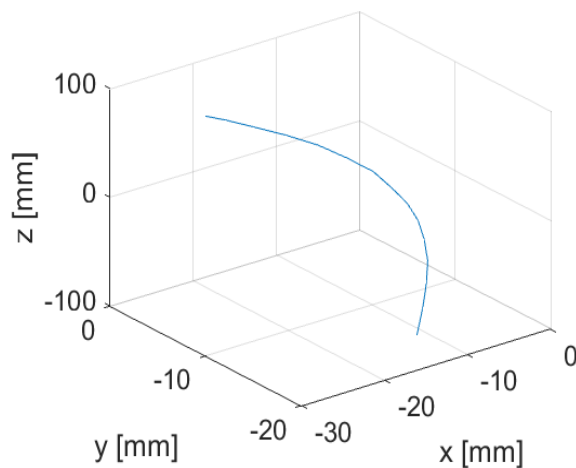


Figure 4.16: Blade trajectory for $\lambda = 5$

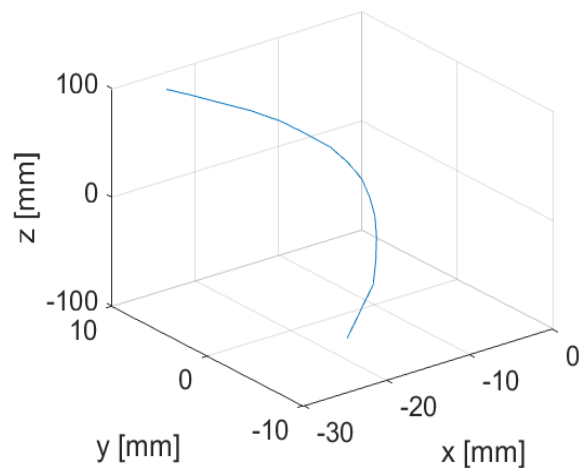
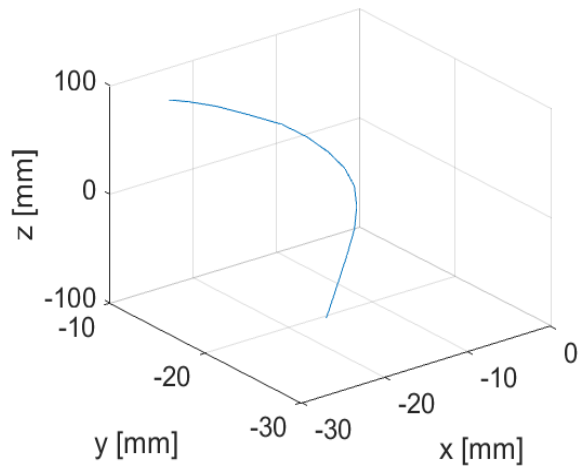
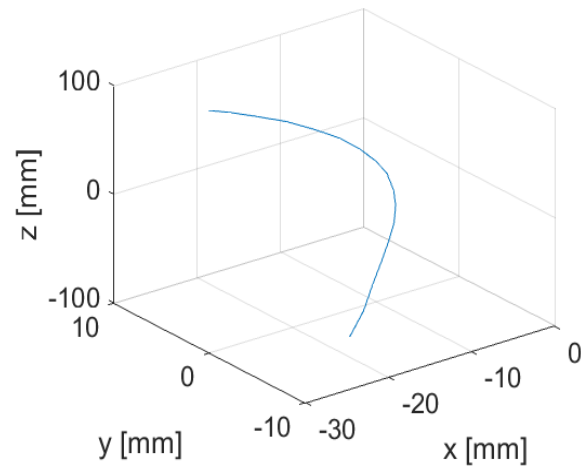
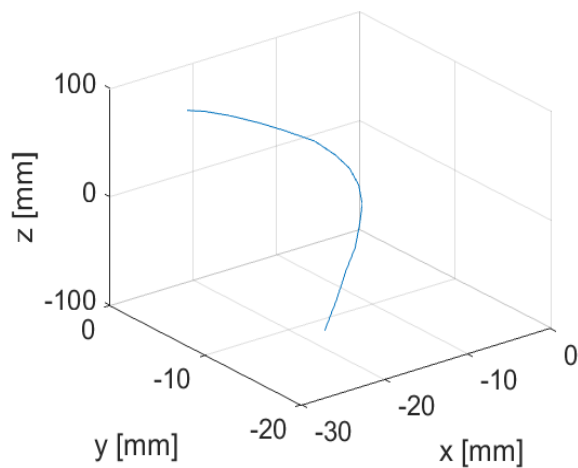
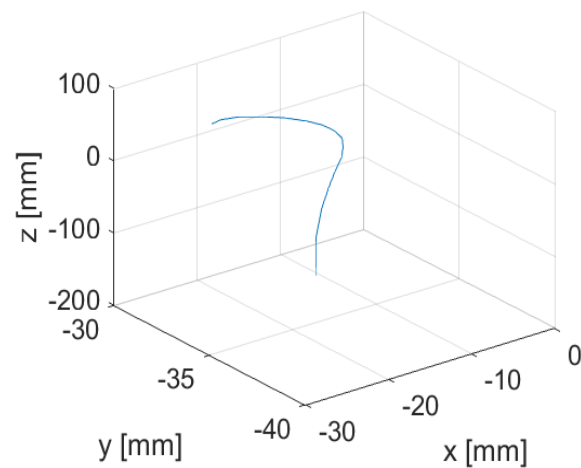


Figure 4.17: Blade trajectory for $\lambda = 6$

Figure 4.18: Blade trajectory for $\lambda = 7$ Figure 4.19: Blade trajectory for $\lambda = 8$ Figure 4.20: Blade trajectory for $\lambda = 9$ Figure 4.21: Blade trajectory for $\lambda = 10$

4.3.2 Vibrations

Based on observations of the blades movement, it was determined that the vibrations were occurring in the z -dimensions (up and down). Thus, this dimension is what is analyzed in order to obtain the most useful data. This was done by analyzing the z -coordinate of the blades trajectory. The z -coordinate should ideally be moving in a linear fashion, since the traversing velocity of the blade is fixed at a specific velocity. The trajectory of the blade in the z -direction is therefore compared to an ideal linear curve, in order to potentially find some discrepancies. The

ideal linear curve is found by fitting a linear curve to the z-coordinate data. This estimation of the ideal trajectory is denoted "Regression Line" in the plots.

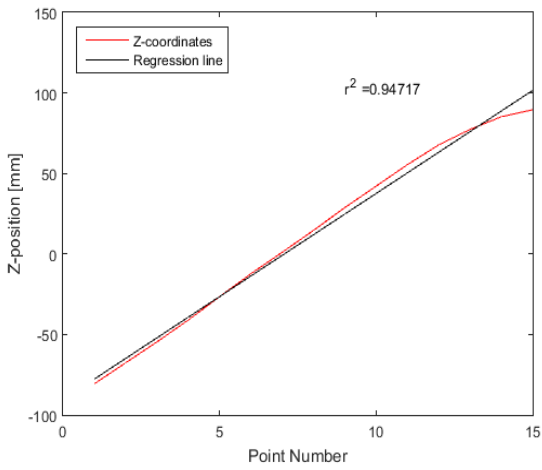


Figure 4.22: Blade movement in z-direction for $\lambda = 5$

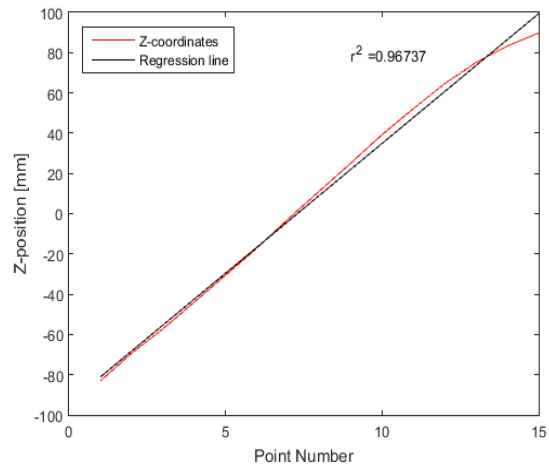


Figure 4.23: Blade movement in z-direction for $\lambda = 6$

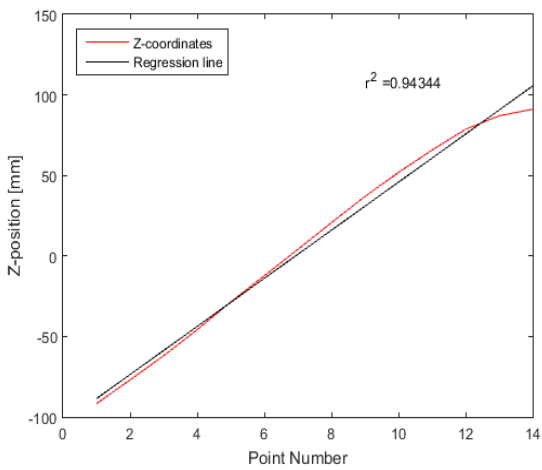


Figure 4.24: Blade movement in z-direction for $\lambda = 7$

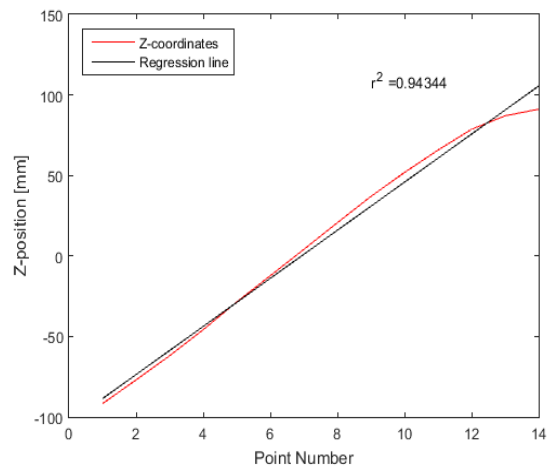


Figure 4.25: Blade movement in z-direction for $\lambda = 8$

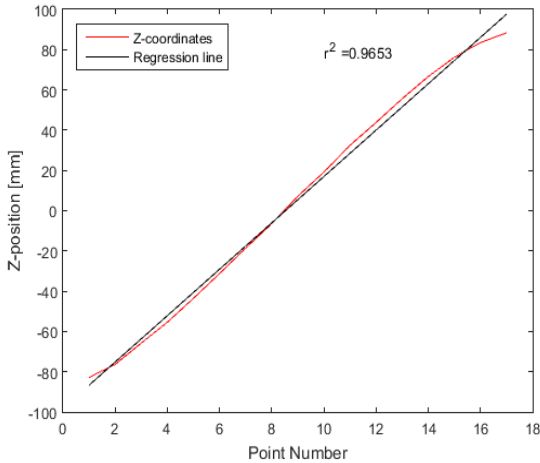


Figure 4.26: Blade movement in z-direction for $\lambda = 9$

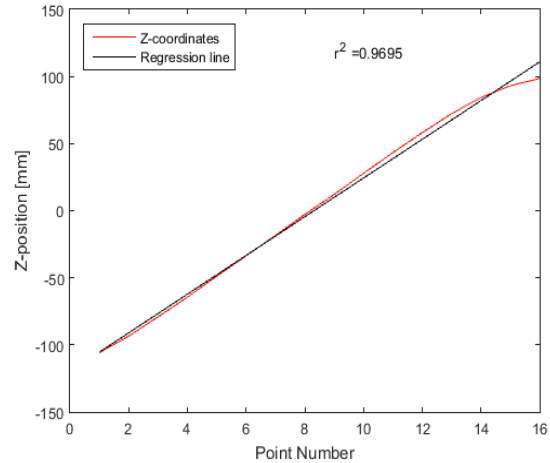


Figure 4.27: Blade movement in z-direction for $\lambda = 10$

4.3.3 Depth of Field Error

As mentioned in section 3.5.2, the camera's focus varies throughout the frame. The cameras were set to focus on the region where the calibration plates were placed. This means that the regions furthest away from the camera (where the blade enters the frame) and closest to the camera (where the blade leaves the frame), where less in focus than the region in the middle.



Figure 4.28: Blade out of focus



Figure 4.29: Blade in focus

This phenomenon becomes clear from figures 4.28 and 4.29. It is obvious that determining the

center of the dot in fig. 4.28, is significantly more challenging than in fig. 4.29. Since both cameras are set to focus on the region where the calibration plates were placed, one would expect the error due lack of camera focus should be smallest in this region of the frame. Typically there were about 15 images per experimental run, where both cameras were able to view the blade at the same time. The error is determined based on the smallest distance between the two camera's lines of sight. Theoretically, the distance between the two lines should be zero (assuming accurate calibration), however, the lack of focus causes an error. The following plot displays this error for $\lambda = 9$:

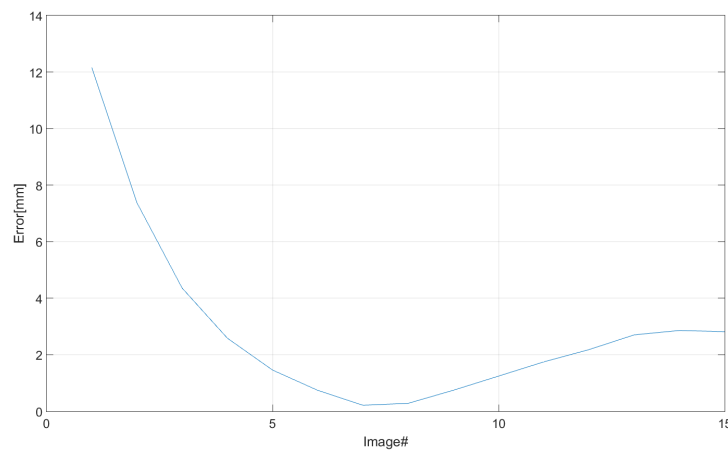


Figure 4.30: Error due to lack of focus

The same tendencies as one can see in fig 4.30 where observable for other λ 's.

4.4 Discussion Regarding Blade Vibrations

Considering the results from this experiment, and comparing it to the problem formulation from section 1.4, one might conclude a partially successful result. The blade trajectory was successfully reconstructed as seen in figures 4.16-4.20. This result proves that the calibration setup as well as the camera setup did indeed work as intended. Further validating the tow tank rig. It also means that the interaction between the cameras also worked, which is useful knowledge for future experiments. The result also validated the method used to obtain the z-coordinate

of the dot on the blade, as laid out in section 3.5.2. Including the MATLAB code used for this purpose. There was however, some issues with reconstructing the trajectory for $\lambda = 10$ as seen in fig 4.21. This might be due to an issue with synchronizing the cameras, yielding some of the later data points to have substantial errors. It is difficult to know for sure, as this was not noticed until the post-processing phase of the thesis. However, since the trajectory was successfully reconstructed for $\lambda = 5 - 9$, as seen in figures 4.16-4.20, one can be confident that the approach is accurate.

However, little valuable information regarding the blade vibrations was obtained. The results displayed in figures 4.22-4.27, yielded little information regarding the nature of the blades vibration. This is likely due to the specifications of the cameras used in this experiments. While the cameras had a maximum frame rate of 3.25 fps, the blade appeared to be vibrating at a frequency significantly higher than this. This makes uncovering information about the vibrations at the tip of the blade quite difficult. Using the exact same method, while simply changing the cameras to some with higher frame rate, would likely yield more information regarding the vibrations. One would also expect that the calibration itself would contain some errors, but since results regarding the nature of the vibration was not obtained, it became somewhat irrelevant.

An interesting finding in this experiment, was the degree to which depth of field was a significant source of error. Considering the results seen in fig. 4.30, and comparing it to figures 4.22-4.27, there appears to be a correlation between the depth of field error, and the discrepancy between the ideal path in the z-direction and the actual data. This result might prove to be helpful in the future, where different lenses could be utilized, as well as adjusting the aperture setting, in order to ensure a larger depth of field, and thus better image focus throughout the movement of the blade. Another option is to only analyze the vibrations in the region of focus for both cameras.

Chapter 5

Conclusions

In this chapter, the work done on this thesis will be summarized and concluded, while keeping in mind the problem formulation from section 1.4. The most important findings from the experiments will be reiterated as well. Furthermore, concrete suggestions for further work will be given, along with reasons why this work would improve upon the work done already in this thesis.

5.1 Conclusion

The overall goal of the thesis was to assess the performance of the new tow tank rig. To accomplish this, the first obstacle was creating a LabVIEW program able to control the two stepper motors. This goal was accomplished. The program performs as intended, allowing the user complete control over the blades traversing and rotational velocities, while also taking important safety concerns into considerations. If used properly, the program should ensure that the blade never traverses to a point where it crashes into either the ceiling or the floor, and potentially harming the rig. The program also has an easy to understand user interface, making it easy to use for people who are new to tow tank rig. Hopefully, this is a program that can be used throughout the lifetime of the tow tank rig.

The second task in order to properly asses the rig was performing a flow visualization experi-

ment. The experiment was largely successful, yielding interesting images of the tip vortices as well as the starting vortices. This experiment proved that performing tip vortex flow visualization, is indeed possible using the tow tank rig. The experiment also showed the expected result, that the vortices were indeed weakened by increasing λ , although this conclusion needs to be taken with a grain of salt for reasons explained in 4.2, it is at the very least an interesting and expected result. Further conclusions regarding the nature of the vortices were not obtainable from this experiment, and is something that should certainly be pursued in future experiments.

The last experiment performed in this thesis, was a blade tracking experiment. This was done to analyze the trajectory of the blade while it traverses and rotates in the tank, as well as to quantify the degree to which the blade is vibrating. Although the experiment was successful in determining the trajectory, it was unsuccessful in obtaining information regarding the vibrations. This is likely due to inefficiencies in the in the cameras as explained in section 4.4. The results from this experiment did however show the importance of camera focus, and the errors that may arise due to lack thereof. Locating the center of the dot proved significantly more difficult when the image was out of focus.

When all is said and done, the overall goal of validating the rig was largely accomplished. One may conclude that it certainly is possible to conduct flow visualization experiments using the blade tow tank. The stepper motor and LabVIEW program allow the researcher to safely and predictably move the blade throughout the tank. However, some flaws have also been uncovered while working on this thesis. There is almost certainly a mechanical issue, causing the blade to vibrate. The blade vibration is something that can be viewed by anyone that watches the blade traverse throughout the tank. This vibration is a source of error in future experiments, if not fixed. The dye injection system was certainly also not optimal. A better system for injecting the dye into the flow could prove valuable in future experiments.

5.2 Further Work

As this thesis is the first work ever to be done on this rig, there is an obvious potential for future research projects. There are however, some improvements should be made to the rig first, in

order to ensure more accurate and reliable results.

5.2.1 Water Quality

For some unknown reason, the water used has a distinct green color. This diminishes the potential quality of any images taken. With green instead of clear water, there is less contrast to work with, and thus harder to obtain valuable information from images taken in the tank. Although much work has already been done to diagnose the problem as well as improve the water quality (with some success), this effort should continue, as it will improve the results from virtually all possible future experiments. For this thesis, the poor water quality made the use of dye very difficult and is the main reason milk was utilized as a substitute.

5.2.2 Blade Shape

Another improvement to the rig would be to use a blade that more closely resembles that of real life wind turbine. This would yield more realistic results, and make it easier to compare results to other researchers. In the long term, it would be interesting to not only test a variety of different airfoils, but also for instance helicopter and ship propellers. The Tow Tank could certainly be used for research on those topics as well.

5.2.3 Blade Vibration

An attempt to analyze the blade vibration should be done. This goal should be obtainable quite quickly. One might use the same procedure as described in this thesis, while getting hold of cameras with a higher frame rate than the ones used in this experiment, in order to likely obtain quantitative data regarding the vibration. After one has obtained a reliable method of determining the vibrations, one can begin troubleshooting in order to find the cause of the problem. A first step could be to remove the outer shaft, to see whether or not friction between the shaft might be a contributing factor. Figuring out the cause of the blade vibration, as well as fixing the problem, is a logical first step, as these effects virtually all experiments conducted in the tank.

5.2.4 Dye Injection

There is potential for improving the system for injecting dye. A good solution would be to implement some kind of pressurized container. This would yield a more manageable and reliable situation, as the dye could be injected into the flow with a precise and reliable velocity. Another advantage of using a pressurized container, would be that outflow velocity of the dye could be easily changed by adjusting the pressure.

On a more practical note, a quicker way to empty and fill the tank would prove useful for future experiments containing dye. Since the dye quickly contaminates the water, by making it less clear, the water needs to be changed often in order to have clear water while taking images. As of now, it takes roughly 30 minutes emptying the tank and almost one hour filling it. This process eats up valuable time that could be spent conducting experiments.

5.2.5 Future Research

With all the practical fixes out of the way, there are a plethora of possibilities that can be explored further. One interesting experiment would be to inject dye into the tank from both blades, and analyzing the interaction between the tip vortices from each blade. This could yield useful information regarding how the wake behind a wind turbine breaks down.

Another interesting research project would be to analyze the wake structure for various configurations of λ , α and blades. This could potentially yield results that will improve wind farm efficiency.

Bibliography

- [1] Global Wind Energy Council. Global statistics, 2016. URL <http://www.gwec.net/global-figures/graphs/>. Online; accessed 30-4-2017.
- [2] National Oceanic and Atmospheric Administration. In the wake of a wind turbine, 2017. URL http://www.noaanews.noaa.gov/stories2011/20110426_windwakes.html. Online; accessed 4-5-2017.
- [3] WikiPedia. Betz's law, 2016. URL https://en.wikipedia.org/wiki/Betz's_law. Online; accessed 7-10-2016.
- [4] Suzan Snow. Wind power is the conversion of wind energy into a useful form, such as electricity, using wind turbines. at the end of 2008, worldwide nameplate capacity, 2016. URL <http://slideplayer.com/slide/6371625/>. Online; accessed 14-10-2016.
- [5] Maryam Refan and Horia Hangan. Aerodynamic performance of a small horizontal axis wind turbine, 2016. URL <http://solarenergyengineering.asmedigitalcollection.asme.org/article.aspx?articleid=1458873>. Online; accessed 15-10-2016.
- [6] Sandia National Laboratories. 2014 sandia wind turbine blade workshop- maniaci, 2014. URL <http://www.slideshare.net/sandiaecis/maniaci-38936527>. Online; accessed 14-10-2016.
- [7] P.H. Alfredsson and J.Å. Dahlberg. A preliminary wind tunnel study of windmill wake dispersion in various flow conditions. *Tech. note AU-1499 7*, 1979. URL https://books.google.no/books/about/A_Preliminary_Wind_Tunnel_Study_of_Windm.html?id=BAX4jwEACAAJ&redir_esc=y.

- [8] Hui Hu, Zifeng Yang, and Partha Sarkar. Dynamic wind loads and wake characteristics of a wind turbine model in an atmospheric boundary layer wind. *Experiments in fluids*, 52(5): 1277–1294, 2012.
- [9] Wikipedia. Osborne reynolds, 2016. URL https://en.wikipedia.org/wiki/Osborne_Reynolds. Online; accessed 29-10-2016.
- [10] Guoquan Jiang and Cuijun Zhao. Camera calibration based on polynomial fitting. In *Computational Intelligence and Software Engineering (CiSE), 2010 International Conference on*, pages 1–4. IEEE, 2010.
- [11] Wind Energy Is Competitive. solutionwind, 2016. URL <http://www.solutionwind.com/blog/wind-energy-is-competitive/>. Online; accessed 17-4-2017.
- [12] Statkraft. Bygger Europas største vindkraftprosjekt i midt-norge, 2016. URL <http://statkraft.no/IR/Stock-Exchange-Notices/2016/bygger-europas-storste-vindkraftprosjekt--i-midt-norge--/>. Online; accessed 4-3-2017.
- [13] Energiwende. Energy transition, 2017. URL <https://energytransition.org/>. Online; accessed 3-5-2017.
- [14] EPA. Energy independence, 2017. URL <https://www.epa.gov/Energy-Independence>. Online; accessed 3-5-2017.
- [15] Office of Energy Efficiency & Renewable Energy. Energy incentive programs, california, 2017. URL <https://energy.gov/eere/femp/energy-incentive-programs-california>. Online; accessed 2-6-2017.
- [16] Wind Measurements International. Wake effects, 2017. URL <http://www.windmeasurementinternational.com/wind-analysis/wake-effects.php>. Online; accessed 20-5-2017.
- [17] A. Crespo L.J. Vermeer, J.N. Sørensenb. Wind turbine wake aerodynamics. *Progress in Aerospace Sciences*, 2003.

- [18] Benjamin Sanderse, SP Pijl, and B Koren. Review of computational fluid dynamics for wind turbine wake aerodynamics. *Wind energy*, 14(7):799–819, 2011.
- [19] Pierre-Elouan Mikael Réthoré. Wind turbine wake in atmospheric turbulence. *Risø National Laboratory for Sustainable Energy*, 2009.
- [20] VL Okulov, IV Naumov, Robert Flemming Mikkelsen, and Jens Nørkær Sørensen. Wake effect on a uniform flow behind wind-turbine model. In *Journal of Physics: Conference Series*, volume 625, page 012011. IOP Publishing, 2015.
- [21] P Fraunie, C Beguier, I Paraschivoiu, and G Brochier. Water channel experiments of dynamic stall on darrieus wind turbine blades. *Journal of Propulsion and Power*, 2(5):445–449, 1986.
- [22] Jenny Marie Bjørnsgaard. Study of wind turbine wake aerodynamics through the application of motion tracking techniques. Master's thesis, NTNU, 2016.
- [23] aweo. Size specifications of common industrial wind turbines, 2016. URL <http://www.aweo.org/windmodels.html>. Online; accessed 30-11-2016.
- [24] DJ Sharpe. A general momentum theory applied to an energy-extracting actuator disc. *Wind Energy*, 7(3):177–188, 2004.
- [25] Grant Ingram. Wind turbine blade analysis using the blade element momentum method. version 1.0. *School of Engineering, Durham University, UK*, 2005.
- [26] Su Liu and Isam Janajreh. Development and application of an improved blade element momentum method model on horizontal axis wind turbines. *International Journal of Energy and Environmental Engineering*, 3(1):1–10, 2012.
- [27] LEM Lignarolo, D Ragni, F Scarano, CJ Simão Ferreira, and GJW van Bussel. Tip-vortex instability and turbulent mixing in wind-turbine wakes. *Journal of Fluid Mechanics*, 781:467–493, 2015.

- [28] Gerardus Joseph Wilhelmus Van Bussel. *The aerodynamics of horizontal axis wind turbine rotors explored with asymptotic expansion methods*. TU Delft, Delft University of Technology, 1995.
- [29] S Hauptmann, M Bülk, L Schön, S Erbslöh, K Boorsma, F Grasso, M Kühn, and PW Cheng. Comparison of the lifting-line free vortex wake method and the blade-element-momentum theory regarding the simulated loads of multi-mw wind turbines. In *Journal of Physics: Conference Series*, volume 555, page 012050. IOP Publishing, 2014.
- [30] Princeton University. Drag of blunt bodies and streamlined bodies, N/A. URL http://www.princeton.edu/~asmits/Bicycle_web/blunt.html. [Online; accessed 24-November-2016].
- [31] Rebecca Jane Barthelmie, SC Pryor, Sten Tronæs Frandsen, Kurt Schaldemose Hansen, JG Schepers, K Rados, W Schlez, A Neubert, LE Jensen, and S Neckelmann. Quantifying the impact of wind turbine wakes on power output at offshore wind farms. *Journal of Atmospheric and Oceanic Technology*, 27(8):1302–1317, 2010.
- [32] Stefan Ivanell, Robert Mikkelsen, Jens N Sørensen, and Dan Henningson. Stability analysis of the tip vortices of a wind turbine. *Wind Energy*, 13(8):705–715, 2010.
- [33] energypedia. Layout of wind projects, 2017. URL https://energypedia.info/wiki/Layout_of_Wind_Projects. Online; accessed 13-6-2017.
- [34] Ylva Odemark and Jens HM Fransson. The stability and development of tip and root vortices behind a model wind turbine. *Experiments in fluids*, 54(9):1–16, 2013.
- [35] Michael Sherry, John Sheridan, and David Lo Jacono. Characterisation of a horizontal axis wind turbine’s tip and root vortices. *Experiments in fluids*, 54(3):1–19, 2013.
- [36] Kurt S Hansen, Rebecca J Barthelmie, Leo E Jensen, and Anders Sommer. The impact of turbulence intensity and atmospheric stability on power deficits due to wind turbine wakes at horns rev wind farm. *Wind Energy*, 15(1):183–196, 2012.

- [37] Neha Marathe, Andrew Swift, Brian Hirth, Richard Walker, and John Schroeder. Characterizing power performance and wake of a wind turbine under yaw and blade pitch. *Wind Energy*, 2015.
- [38] Alexander J Smits. *Flow visualization: techniques and examples*. World Scientific, 2012.
- [39] Bruno Eckhardt. Introduction. turbulence transition in pipe flow: 125th anniversary of the publication of reynolds' paper. *Philosophical Transactions of the Royal Society of London A: Mathematical, Physical and Engineering Sciences*, 367(1888):449–455, 2009.
- [40] dantecdynamics. Measurement principles of piv, 2016. URL <http://www.dantecdynamics.com/measurement-principles-of-piv>. Online; accessed 1-11-2016.
- [41] JH Strickland, BT Webster, and T Nguyen. A vortex model of the darrieus turbine: an analytical and experimental study. *Journal of Fluids Engineering*, 101(4):500–505, 1979.
- [42] L.J. Clancy. *Aerodynamics*. Pitman Aeronautical Engineering Series. Wiley, 1975. ISBN 9780470158371. URL <https://books.google.no/books?id=zaNTAAAMAAJ>.
- [43] Jan Bartl and Lars Sætran. Blind test comparison of the performance and wake flow between two in-line wind turbines exposed to different turbulent inflow conditions. *Wind Energy Science*, 2(1):55–76, 2017.
- [44] Advanced Micro Systems. Stepper motor system basics, 2016. URL http://www.stepcontrol.com/stepping101/stepping101_Motors_6.html. Online; accessed 15-2-2017.
- [45] adafruit. What is a stepper motor?, 2016. URL <https://learn.adafruit.com/all-about-stepper-motors/what-is-a-stepper-motor>. Online; accessed 29-11-2016.
- [46] Imperx. B4820, 2017. URL <http://www.imperx.com/ccd-cameras/b4820/>. Online; accessed 28-5-2017.
- [47] National Instruments. Labview system design software, 2016. URL <http://www.ni.com/labview/>. Online; accessed 25-11-2016.

- [48] Darren Rowse. Introduction to aperture in digital photography, 2017. URL <https://digital-photography-school.com/aperture/>. Online; accessed 13-4-2017.
- [49] MIT. Dye injection;, 2016. URL http://web.mit.edu/fluids-modules/www/exper_techniques/2.Dye_Injection.pdf. Online; accessed 21-02-2017.
- [50] T. T. Lim. *Flow Visualization: Techniques and Examples*. Imperial College Press, 2000.
- [51] fao. Properties of milk, 2017. URL <http://www.fao.org/ag/AGInfo/themes/documents/Dairyman/Dairy/V1U1p1.htm>. Online; accessed 13-6-2017.

Appendix A

Matlab Scripts

A.1 Calculating Z-coordinate

A.2 MATLAB Scripts

```
close all
clear all
clc

images = {imread('bladeLeft.bmp'), imread('bladeRight.bmp')};
zoom_size = 600;
pixnum=size(images{1});
boxs=45;

%im = im < 60;
for i = 1:length(images)
    imagesc(images{i})
    title('White part of image')
```

```

[zoomcenx, zoomceny]=ginput(1);
xlim([zoomcenx-(zoom_size/4) zoomcenx+(zoom_size/4)]), ...
ylim([zoomceny-(zoom_size/4) zoomceny+(zoom_size/4)])
[zoomcenx, zoomceny]=ginput(1);
x1=floor(zoomcenx-(boxs/2));
x2=ceil(zoomcenx+(boxs/2));
y1=floor(zoomceny-(boxs/2));
y2=ceil(zoomceny+(boxs/2));
calData = load(['cal_dat_00' num2str(i) '.txt']);
clipixnum = size(images{i});
poly_n = 3;
x = zoomcenx;
y = zoomceny;
a=clipixnum(2)/2;
b=clipixnum(1)/2;
[sing_clx_pl1(i)]=polynmapping(x,y,a,b,calData(1:10,1),poly_n);
[sing_cly_pl1(i)]=polynmapping(x,y,a,b,calData(1:10,2),poly_n);
[sing_clx_pl2(i)]=polynmapping(x,y,a,b,calData(1:10,3),poly_n);
[sing_cly_pl2(i)]=polynmapping(x,y,a,b,calData(1:10,4),poly_n);
end

close all

point1 = [sing_clx_pl1(1) sing_cly_pl1(1) -1];
point2 = [sing_clx_pl2(1) sing_cly_pl2(1) 0];

point3 = [sing_clx_pl1(2) sing_cly_pl2(2) -1];
point4 = [sing_clx_pl2(2) sing_cly_pl2(2) 0];

scalingFactor = 200;

point5 = [point1(1) + (point1(1) - point2(1))*scalingFactor, ...
point1(2) + (point1(2) - point2(2))*scalingFactor, point1(3) ...
+ (point1(3) - point2(3))*scalingFactor];
point6 = [point2(1) + (point2(1)-point1(1))*scalingFactor, ...

```

```
point2(2) + (point2(2)-point1(2))*scalingFactor, point2(3)...
+ (point2(3)-point1(3))*scalingFactor];

point7 = [point3(1) + (point3(1)-point4(1))*scalingFactor,...
point3(2) + (point3(2)-point4(2))*scalingFactor, point3(3)...
+ (point3(3)-point4(3))*scalingFactor];
point8 = [point4(1) + (point4(1)-point3(1))*scalingFactor,...
point4(2) + (point4(2)-point3(2))*scalingFactor, point4(3)...
+ (point4(3)-point3(3))*scalingFactor];

[dis, m1, m2, m3] = DistBetween2Segment(point5, point6, point7, point8);
zposition = mean([m3(3) m2(3)]);
yposition = mean([m3(2) m2(2)]);
xposition = mean([m3(1) m2(1)]);
intersection = [xposition yposition zposition];

A1 = [sing_clx_pl1(1),sing_clx_pl2(1)];
B1 = [sing_cly_pl1(1), sing_cly_pl2(1)];
A2 = [sing_clx_pl1(2), sing_clx_pl2(2)];
B2 = [sing_cly_pl1(2), sing_cly_pl2(2)];

p1 = polyfit(A1, B1, 1);
p2 = polyfit(A2, B2, 1);
x1 = linspace(A1(1), A1(2), 101);
x2 = linspace(A2(1), A2(2), 101);
y1 = polyval(p1,x1);
y2 = polyval(p2,x2);

figure(2)
plot3([point5(1) point6(1)], [point5(2) point6(2)], [point5(3) point6(3)]);
hold on
plot3([point7(1) point8(1)], [point7(2) point8(2)], [point7(3) point8(3)]);
```

```
xlabel('x')
ylabel('y')
zlabel('z')
```

A.3 Blade Tracking Data

A.4 MATLAB Scripts

```
clear all
close all
clc

%TSR = 5
point1 = [-14.000259232200534,-18.188618914701620,-80.634558379234870];
point2 = [-11.569972742893912,-16.691194147981818,-67.628107237119020];
point3 = [-9.863544500883167,-15.577812340398438,-54.626319340824450];
point4 = [-8.642816284882858,-14.654619166568253,-41.045358531284450];
point5 = [-8.092654072126983,-13.795912886685054,-26.588390322736970];
point6 = [-8.078007254534171,-13.154358888201198,-12.293787224835995];
point7 = [-8.518963945608210,-12.403963461946946,1.021728637095279];
point8 = [-9.578786475303879,-11.689025815367769,14.604212061776096];
point9 = [-10.865642846341590,-10.902429379702303,28.770591876481063];
point10 = [-12.962818686471309,-10.053738505496398,42.078801054544456];
point11 = [-15.402298371662827,-9.120356398620604,55.456487979388260];
point12 = [-18.330700269850320,-8.238756529071384,67.708079648897310];
point13 = [-21.080439209196165,-7.338404365324884,77.337664132636530];
point14 = [-23.442651025195424,-6.436690478066573,85.189344153634950];
point15 = [-25.135155924016810,-5.679488597874336,89.508754056395960];

xcoords = [point1(1), point2(1), point3(1), point4(1), point5(1), point6(1), ...
point7(1), point8(1), point9(1), point10(1), point11(1), ...
```

```

point12(1), point13(1), point14(1), point15(1)];
ycoords = [point1(2), point2(2), point3(2), point4(2), point5(2), point6(2)...
, point7(2), point8(2), point9(2), point10(2), point11(2), point12(2)...
, point13(2), point14(2), point15(2)];
zcoords = [point1(3), point2(3), point3(3), point4(3), point5(3), point6(3)...
, point7(3), point8(3), point9(3), point10(3), point11(3), point12(3)...
, point13(3), point14(3), point15(3)];

```

```

figure(1)
plot3(xcoords, ycoords, zcoords);
xlabel('x [mm]')
ylabel('y [mm]')
zlabel('z [mm]')
set(gca, 'fontsize', 18)
grid on

```

```

polyTSR5 = polyfit(1:15, zcoords, 1);
for i = 1:15
    regressionTSR5(i) = polyval(polyTSR5, i);
end

```

```

figure(2)
plot(1:15, zcoords, 'r', 1:15, regressionTSR5, 'k')
xlabel('Point Number')
ylabel('Z-position [mm]')
legend('Z-coordinates', 'Regression line', 'Location', 'northwest')
set(gca, 'fontsize', 18)
[polyTSR5, errTSR5] = polyfit(1:15, zcoords, 1);
rquaredTSR5 = 1-errTSR5.normr^2/norm(polyTSR5 -mean(polyTSR5))^2;
text(9, 105, ['r^2 = ' num2str(rquaredTSR5)])

```

```

%TSR = 6
point1 = [-19.570051771757242, -5.513283932206676, -83.123111996357700];
point2 = [-11.879807973659481, -1.562923387061600, -69.286585441528270];

```

```
point3 = [-9.957579116293712,-0.167717860033154,-57.260870216835570];
point4 = [-8.644382098415987,0.912758720626246,-43.932270657708710];
point5 = [-7.949049180170986,1.684658002078673,-30.538369133540130];
point6 = [-7.726299351259106,2.416433461781321,-17.127615553438970];
point7 = [-7.983055006318945,3.028159945381606,-2.660243220451434];
point8 = [-8.848983529558216,3.694453995390000,11.280948896124244];
point9 = [-10.126752258113726,4.429941700554700,25.067168739397403];
point10 = [-12.269135802472892,5.200163121128512,39.318801276378880];
point11 = [-14.402354433645993,6.012718347998725,52.180707603009950];
point12 = [-17.126282278604045,6.792263550508821,64.612280125800240];
point13 = [-20.017877160038427,7.647208467168929,75.098083951931900];
point14 = [-22.300908800870660,8.425307813770960,83.324480890338760];
point15 = [-24.356818032512262,9.248459553871516,89.729202949060640];
```

```
xcoords = [point1(1), point2(1), point3(1), point4(1), point5(1) ...
, point6(1), point7(1), point8(1), point9(1), point10(1), ...
point11(1), point12(1), point13(1), point14(1), point15(1)];
ycoords = [point1(2), point2(2), point3(2), point4(2), point5(2), ...
point6(2), point7(2), point8(2), point9(2), point10(2), ...
point11(2), point12(2), point13(2), point14(2), point15(2)];
zcoords = [point1(3), point2(3), point3(3), point4(3), point5(3), ...
point6(3), point7(3), point8(3), point9(3), point10(3), ...
point11(3), point12(3), point13(3), point14(3), point15(3)];
```

```
figure(3)
plot3(xcoords, ycoords, zcoords);
xlabel('x [mm]')
ylabel('y [mm]')
zlabel('z [mm]')
set(gca, 'fontsize', 18)
grid on

polyTSR6 = polyfit(1:15, zcoords, 1);
for i = 1:15
```



```

    regressionTSR6(i) = polyval(polyTSR6,i);
end

figure(4)
plot(1:15, zcoords, 'r', 1:15, regressionTSR6, 'k')
xlabel('Point Number')
ylabel('Z-position [mm]')
legend('Z-coordinates', 'Regression line', 'Location', 'northwest')
set(gca, 'fontsize', 18)
[polyTSR6, errTSR6] = polyfit(1:15, zcoords, 1);
rquaredTSR6 = 1-errTSR6.normr^2/norm(polyTSR6 -mean(polyTSR6))^2;
text(9,80, ['r^2 =' num2str(rquaredTSR6)])

%TSR = 7
point1 = [-17.042029753297726, -21.364061074709504, -91.686959388503080];
point2 = [-13.426973127475620, -19.431831327916720, -76.966217461613010];
point3 = [-11.022147967147250, -18.292842745552220, -61.940884028902500];
point4 = [-9.312669100578399, -17.568703304174694, -45.822533285565440];
point5 = [-8.501144472206946, -17.107083690165510, -28.581390139835776];
point6 = [-8.349540834700868, -16.723125629051665, -12.281021511547337];
point7 = [-9.062100433951489, -16.338421749903418, 4.064834950784402];
point8 = [-10.554648467607553, -15.892813259064091, 20.643265710006986];
point9 = [-12.565421123271271, -15.400628927695768, 36.957551150078230];
point10 = [-14.989110274545883, -14.911330257253920, 51.822364042096766];
point11 = [-18.309147479525250, -14.332086702853350, 65.732144929652630];
point12 = [-21.560044541561037, -13.756392648723603, 78.627108715796310];
point13 = [-24.335335340914824, -13.272512913551523, 87.001938036426510];
point14 = [-26.183476913793346, -12.843202928348020, 91.134246021007910];

xcoords = [point1(1), point2(1), point3(1), point4(1), point5(1), ...
point6(1), point7(1), point8(1), point9(1), point10(1), ...
point11(1), point12(1), point13(1), point14(1)];
ycoords = [point1(2), point2(2), point3(2), point4(2), point5(2), ...
point6(2), point7(2), point8(2), point9(2), point10(2), ...
point11(2), point12(2), point13(2), point14(2)];

```

```
zcoords = [point1(3), point2(3), point3(3), point4(3), point5(3), ...
point6(3), point7(3), point8(3), point9(3), point10(3), ...
point11(3), point12(3), point13(3), point14(3)];
```

```
figure(5)
plot3(xcoords, ycoords, zcoords);
xlabel('x [mm]')
ylabel('y [mm]')
zlabel('z [mm]')
set(gca, 'fontsize', 18)
grid on
```

```
polyTSR7 = polyfit(1:14, zcoords, 1);
for i = 1:14
    regressionTSR7(i) = polyval(polyTSR7, i);
end
```

```
figure(6)
plot(1:14, zcoords, 'r', 1:14, regressionTSR7, 'k')
xlabel('Point Number')
ylabel('Z-position [mm]')
legend('Z-coordinates', 'Regression line', 'Location', 'northwest')
set(gca, 'fontsize', 18)
[polyTSR7, errTSR7] = polyfit(1:14, zcoords, 1);
rquaredTSR7 = 1 - errTSR7.normr^2 / norm(polyTSR7 - mean(polyTSR7))^2;
text(9, 110, ['r^2 = ' num2str(rquaredTSR7)])
```

```
%TSR = 8
point1 = [-19.782257761099164, -5.754652981928175, ...
-82.815321085467530, 11.149791222135521];
point2 = [-15.990512450830845, -3.908382040658026, ...
-76.314613262984980, 7.182798377346792];
point3 = [-13.092373472239501, -2.349269624026184, ...
-65.767663420906220, 4.290075107433617];
point4 = [-10.880709029779208, -1.311737062567230, ...
```

```
-55.394891897755116, 2.527156620902633];
point5 = [-9.157104746888287,-0.593769397079760,...
-43.538159244214670, 1.444106014959441];
point6 = [-7.929317305291673,-0.104686723894007,...
-31.230261027942646, 0.764526064431911];
point7 = [-7.287533091501016,0.299357585697674,...
-18.639780237327955, 0.304847803968719];
point8 = [-7.150547534964531,0.639121761223451,...
-6.439778458906190, 0.061502144538008];
point9 = [-7.432840854885361,1.080262959730997,...
7.180940389542158, 0.269441199248649];
point10 = [-8.346210995703120,1.430462740014036,...
19.180877295437910, 0.532781817268838];
point11 = [-9.898343013637245,1.868720608740062,...
32.473041380857810, 0.898368480401062];
point12 = [-11.646250631411434,2.319623669219465,...
43.835399580262220, 1.220253501410769];
point13 = [-14.169791683285652,2.791646668390293,...
55.628324830563460, 1.391393643616855];
point14 = [-16.864950811627060,3.347552304781982,...
66.644032814610580, 1.593510871292419];
point15 = [-19.886418908410153,3.839194609933990,...
76.200491783171320, 1.823449579464164];
point16 = [-22.444123916493260,4.344104561001037,...
83.509405348423940, 1.943480650840622];
point17 = [-24.603582246457968,4.838182067716308,...
88.340154456519810, 1.908324931590473];

xcoords = [point1(1), point2(1), point3(1), point4(1), point5(1),point6(1),...
point7(1), point8(1), point9(1), point10(1), point11(1), point12(1),...
point13(1), point14(1), point15(1), point16(1), point17(1)];
ycoords = [point1(2), point2(2), point3(2), point4(2), point5(2), point6(2),...
point7(2), point8(2), point9(2), point10(2), point11(2), point12(2),...
point13(2), point14(2), point15(2), point16(2), point17(2)];
```

```

zcoords = [point1(3), point2(3), point3(3), point4(3), point5(3), point6(3),...
point7(3), point8(3), point9(3), point10(3), point11(3), point12(3),...
point13(3), point14(3), point15(3), point16(3), point17(3)];
errors = [point1(4), point2(4), point3(4), point4(4), point5(4), point6(4),...
point7(4), point8(4), point9(4), point10(4), point11(4), point12(4),...
point13(4), point14(4), point15(4), point16(4), point17(4)];

```

```

figure(7)
plot3(xcoords, ycoords, zcoords);
xlabel('x [mm]')
ylabel('y [mm]')
zlabel('z [mm]')
set(gca, 'fontsize', 18)
grid on

```

```

polyTSR8 = polyfit(1:17, zcoords, 1);
for i = 1:17
    regressionTSR8(i) = polyval(polyTSR8, i);
end

```

```

figure(8)
plot(1:17, zcoords, 'r', 1:17, regressionTSR8, 'k')
xlabel('Point Number')
ylabel('Z-position [mm]')
legend('Z-coordinates', 'Regression line', 'Location', 'northwest')
set(gca, 'fontsize', 18)
[polyTSR8, errTSR8] = polyfit(1:17, zcoords, 1);
rquaredTSR8 = 1-errTSR8.normr^2/norm(polyTSR8 - mean(polyTSR8))^2;
text(10, 80, ['r^2 = ' num2str(rquaredTSR8)])

```

```

figure(9)
plot(1:17, errors)
xlabel('Image#')
ylabel('Error[mm]')
set(gca, 'fontsize', 18)
grid on

```

```
%TSR = 9
point1 = [-18.763595317148585,-12.678543719011714,...
-91.373987205770820, 12.161741840918518];
point2 = [-14.784838640568388,-10.503403607107959,...
-81.176005153036610, 7.375445787212898];
point3 = [-12.085979037948768,-9.087200705823768,...
-68.509186861605060, 4.357558206398839];
point4 = [-10.088718264542358,-8.320632311168845,...
-55.130442086672630, 2.586971996355425];
point5 = [-8.833896647484064,-7.711538246485367,...
-38.850776562891480, 1.459206028724640];
point6 = [-8.168284392118348,-7.389703944656686,...
-23.767795404070880, 0.742462012048881];
point7 = [-8.258656846384762,-7.101959680302436,...
-7.579732314989286, 0.214691585378021];
point8 = [-9.092283208840290,-6.875344122392423,...
8.878016414680076, 0.283911293449174];
point9 = [-10.467901062761566,-6.575834401213589,...
23.077314534816182, 0.746756134193609];
point10 = [-12.495230355965106,-6.216652341336358,...
38.753483402287160, 1.247022116833085];
point11 = [-15.460919387305860,-5.776047879260727,...
53.103164496619684, 1.749754409728054];
point12 = [-18.321029655297572,-5.448635669146047,...
65.912812236893340, 2.183300260643653];
point13 = [-21.412603029094345,-5.016448099728763,...
77.937802516089020, 2.705271358086700];
point14 = [-24.009355969157696,-4.667773351841909,...
86.286725783775350, 2.859616742236105];
point15 = [-25.877308027268070,-4.365971333451274,...
90.211931528341410, 2.818031687394802];
```

```

xcoords = [point1(1), point2(1), point3(1), point4(1), point5(1),...
point6(1), point7(1), point8(1), point9(1), point10(1),...
point11(1), point12(1), point13(1), point14(1), point15(1)];
ycoords = [point1(2), point2(2), point3(2), point4(2), point5(2),...
point6(2), point7(2), point8(2), point9(2), point10(2),...
point11(2), point12(2), point13(2), point14(2), point15(2)];
zcoords = [point1(3), point2(3), point3(3), point4(3), point5(3),...
point6(3), point7(3), point8(3), point9(3), point10(3),...
point11(3), point12(3), point13(3), point14(3), point15(3)];
errors = [point1(4), point2(4), point3(4), point4(4), point5(4),...
point6(4), point7(4), point8(4), point9(4), point10(4),...
point11(4), point12(4), point13(4), point14(4), point15(4)];

figure(10)
plot3(xcoords, ycoords, zcoords);
xlabel('x [mm]')
ylabel('y [mm]')
zlabel('z [mm]')
set(gca, 'fontsize', 18)
grid on

polyTSR9 = polyfit(1:15, zcoords, 1);
for i = 1:15
    regressionTSR9(i) = polyval(polyTSR9, i);
end

figure(11)
plot(1:15, zcoords, 'r', 1:15, regressionTSR9, 'k')
xlabel('Point Number')
ylabel('Z-position [mm]')
legend('Z-coordinates', 'Regression line', 'Location', 'northwest')
set(gca, 'fontsize', 18)
[polyTSR9, errTSR9] = polyfit(1:15, zcoords, 1);
rquaredTSR9 = 1 - errTSR9.normr^2 / norm(polyTSR9 - mean(polyTSR9))^2;
text(9, 115, ['r^2 = ' num2str(rquaredTSR9)])

```

```
figure(12)
plot(1:15, errors)
xlabel('Image#')
ylabel('Error[mm]')
set(gca, 'fontsize', 18)
grid on

%TSR = 10
point1 = [-20.369692206975017, -36.344953384772300, ...
-1.057354657976161e+02, 15.200674261395218];
point2 = [-16.149141624215880, -34.532025163473655, ...
-93.490738409821090, 9.900393203581578];
point3 = [-12.959034832004514, -33.442830436498646, ...
-79.116070898194120, 6.454271800732463];
point4 = [-10.973078627293887, -32.938291504768360, ...
-64.430439492895660, 4.375933137764770];
point5 = [-9.600521399413779, -32.693255027066100, ...
-48.769863227318570, 2.924204789918300];
point6 = [-8.778698001194890, -32.666357509963530, ...
-33.651677574684330, 1.805531753335083];
point7 = [-8.705067036560346, -32.717982276373400, ...
-18.452191493285582, 1.007788411237780];
point8 = [-9.129081857462054, -32.851822856885605, ...
-2.775650970848858, 0.030723676978103];
point9 = [-10.204414736653660, -32.926676762030134, ...
12.099279596910918, 0.836601998284290];
point10 = [-11.927774991885842, -33.057120615044820, ...
27.842822233535912, 1.671729150204619];
point11 = [-14.157004841976933, -33.212613708287414, ...
43.287713400936200, 2.470592214270176];
point12 = [-16.941628104551036, -33.239476867204175, ...
58.106114810821280, 3.279464011173924];
point13 = [-20.033206127144360, -33.371610679303330, ...
72.327202601390720, 4.018724651335128];
point14 = [-23.042972968949530, -33.495206632420704, ...
84.342930736957360, 4.438633306776766];
```

```
point15 = [-25.724619589900570,-33.730698704382110,...
93.096300025577280, 4.716889332903191];
point16 = [-27.599168281937548,-34.062966261915940,...
98.516652262154170, 4.514054476982071];

xcoords = [point1(1), point2(1), point3(1), point4(1), point5(1),...
point6(1), point7(1), point8(1), point9(1), point10(1),...
point11(1), point12(1), point13(1), point14(1), point15(1), point16(1)];
ycoords = [point1(2), point2(2), point3(2), point4(2), point5(2),...
point6(2), point7(2), point8(2), point9(2), point10(2),...
point11(2), point12(2), point13(2), point14(2), point15(2), point16(2)];
zcoords = [point1(3), point2(3), point3(3), point4(3), point5(3),...
point6(3), point7(3),...
point8(3), point9(3), point10(3),...
point11(3), point12(3), point13(3), point14(3), point15(3), point16(3)];

figure(13)
plot3(xcoords, ycoords, zcoords);
xlabel('x [mm]')
ylabel('y [mm]')
zlabel('z [mm]')
set(gca,'fontsize',18)
grid on

polyTSR10 = polyfit(1:16, zcoords,1);
for i = 1:16
    regressionTSR10(i) = polyval(polyTSR10,i);
end

figure(14)
plot(1:16, zcoords, 'r', 1:16, regressionTSR10, 'k')
```



```
xlabel('Point Number')
ylabel('Z-position [mm]')
legend('Z-coordinates', 'Regression line', 'Location', 'northwest')
set(gca, 'fontsize', 18)
[polyTSR10, errTSR10] = polyfit(1:16, zcoords, 1);
rquaredTSR10 = 1-errTSR10.normr^2/norm(polyTSR10 - mean(polyTSR10))^2;
text(9, 120, ['r^2 = ' num2str(rquaredTSR10)])
```

Appendix B

LabVIEW Block Diagram

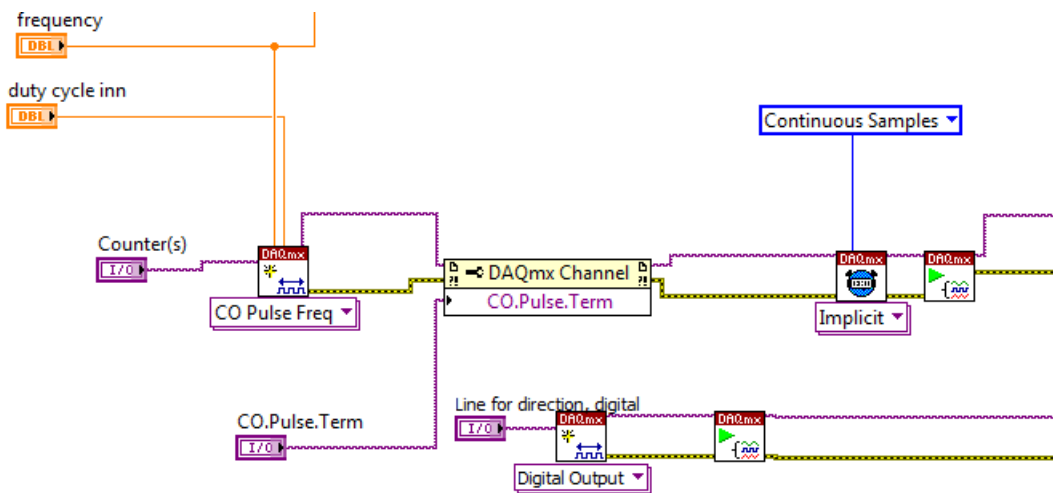


Figure B.1: Signal Generation

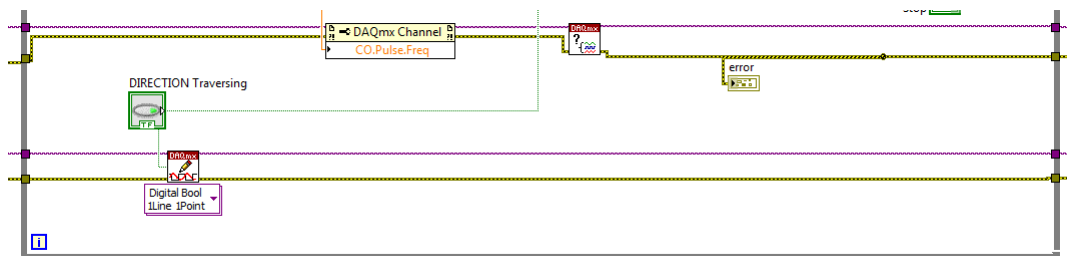


Figure B.2: Pulse in Loop

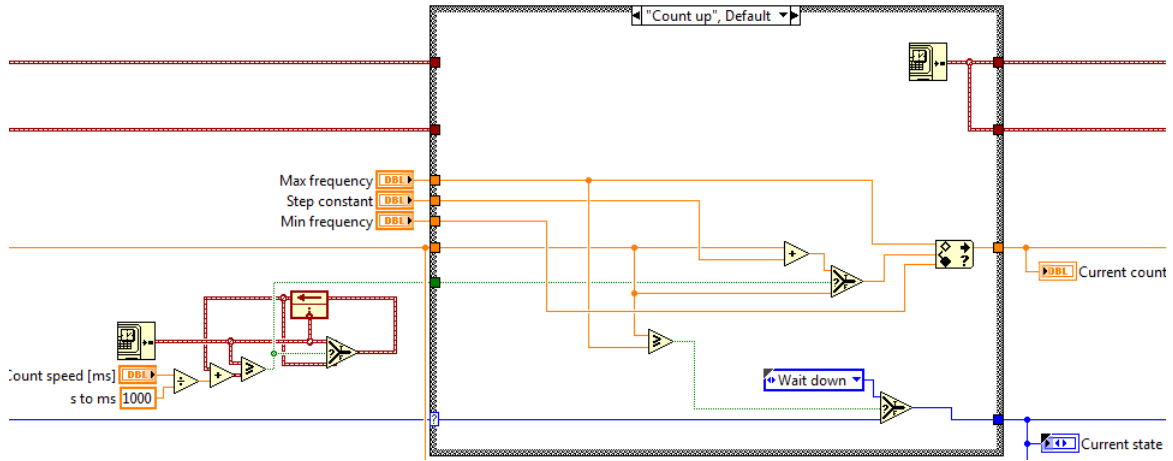


Figure B.3: Acceleration Code

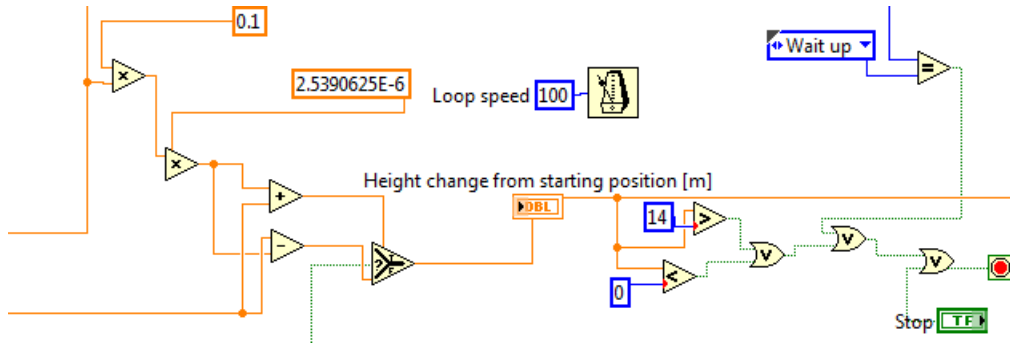


Figure B.4: Safety Features

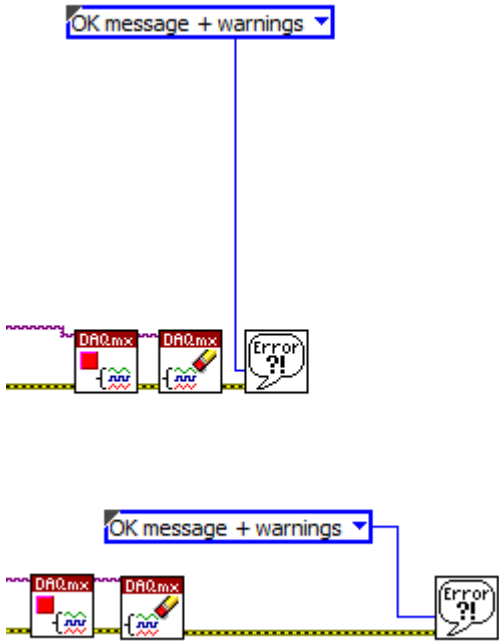


Figure B.5: End of Cycle